NONLINEAR SEISMIC PERFORMANCE EVALUATION OF REINFORCED CONCRETE BUILDINGS USING PUSHOVER ANALYSIS IN SAP2000

(A Self-Initiated Project)

A Project Report

Submitted in partial fulfillment of the requirements for the award of the degree of

Bachelor of Technology

in

Civil Engineering

Submitted by

Aman Paturde
Roll No.: B-223

ABSTRACT

The seismic performance of reinforced concrete (RC) buildings is strongly influenced by structural configuration, stiffness distribution, and the presence of lateral load-resisting systems. Conventional linear analysis methods are unable to adequately capture the inelastic behavior and damage progression that occur during strong earthquake excitation. Therefore, nonlinear static pushover analysis has become an important tool for evaluating structural performance beyond the elastic range.

In the present study, five reinforced concrete building configurations were investigated using SAP2000: a G+15 regular frame, a G+20 regular frame, a G+20 setback (irregular) building, a G+20 core shear wall building, and a G+20 perimeter shear wall building. Linear static analysis, modal analysis, response spectrum analysis, and nonlinear pushover analysis were performed in accordance with IS 1893:2016. Structural performance was evaluated using ATC-40 procedures and FEMA/ASCE hinge models.

The results demonstrated significant variation in seismic behavior among the investigated systems. The regular frame buildings exhibited the highest global ductility, with ductility factors of 4.71 and 5.71 for the G+15 and G+20 models, respectively. The setback building showed concentrated hinge formation near the irregularity level and a reduced derived response reduction factor of 4.07, indicating lower energy dissipation capability. The core shear wall model achieved an overstrength factor of 1.97 and exhibited the smallest performance point displacement, demonstrating superior stiffness and drift control. The perimeter shear wall system provided the highest reserve strength with an overstrength factor of 3.40 and a derived response reduction factor of 16.47, indicating excellent seismic resistance through combined frame-wall interaction.

Comparative evaluation of capacity curves, performance points, hinge formation patterns, ductility, overstrength, and derived response reduction factors showed that shear wall systems substantially improve seismic performance compared with conventional moment-resisting frames. Among the investigated configurations, the perimeter shear wall system exhibited the most favorable overall seismic behavior, while the setback building was found to be the most vulnerable due to stiffness discontinuity and deformation concentration at the setback level.

Keywords: Pushover Analysis, Seismic Performance Evaluation, Reinforced Concrete Buildings, Shear Walls, Structural Irregularity, SAP2000, ATC-40, Nonlinear Static Analysis.

CHAPTER 1
INTRODUCTION

1.1 Background

Earthquakes are among the most destructive natural hazards affecting human life, infrastructure, and economic development. Throughout history, several devastating earthquakes have caused significant damage to buildings and other civil engineering structures due to the large lateral forces generated by ground motion. Reinforced concrete (RC) buildings, which constitute a major portion of modern urban infrastructure, are particularly vulnerable to seismic forces when not adequately designed to withstand them.

The primary objective of seismic design is to ensure that structures possess sufficient strength, stiffness, and ductility to resist earthquake loading without experiencing catastrophic collapse. Conventional seismic design procedures are generally based on linear elastic analysis methods, which assume that the structure remains within the elastic range throughout the loading process. However, during strong earthquakes, structures often undergo inelastic behavior, resulting in cracking, yielding of reinforcement, formation of plastic hinges, and redistribution of internal forces.

Linear analysis techniques such as Equivalent Static Analysis and Response Spectrum Analysis are useful for estimating design forces and overall structural response. However, these methods are unable to accurately predict the actual nonlinear behavior of structures under severe earthquake loading. They cannot identify the sequence of damage, hinge formation patterns, collapse mechanisms, or the reserve strength available beyond the elastic limit.

To overcome these limitations, nonlinear analysis methods have been developed. Among these methods, nonlinear static pushover analysis has become one of the most widely used techniques for seismic performance assessment. Pushover analysis provides valuable information regarding the strength, stiffness, ductility, and deformation capacity of structures by progressively applying lateral loads until significant nonlinear behavior occurs.

The present study focuses on evaluating the nonlinear seismic performance of different reinforced concrete building configurations using pushover analysis. The study investigates the influence of structural irregularity and shear wall systems on the seismic behavior of buildings by comparing regular frame structures, setback structures, core shear wall systems, and perimeter shear wall systems.

Figure 1: Earthquake-damaged reinforced concrete building.

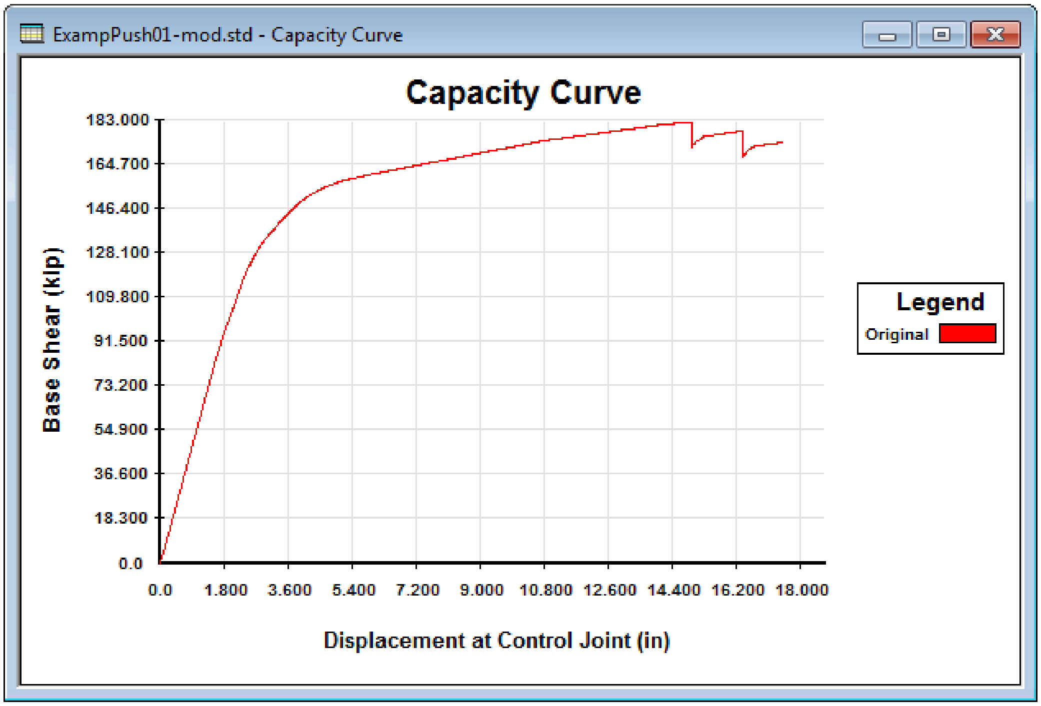

Figure 2: Typical capacity curve obtained from pushover analysis.

1.2 Problem Statement

Most reinforced concrete buildings are designed using linear elastic analysis methods prescribed by seismic design codes. Although these methods provide satisfactory estimates of design forces, they do not accurately represent the actual behavior of structures during strong earthquakes. Structural response under severe seismic loading is inherently nonlinear and involves cracking, yielding, plastic hinge formation, stiffness degradation, and energy dissipation.

Furthermore, buildings with geometric irregularities, such as setbacks and buildings incorporating shear wall systems, exhibit seismic behavior significantly different from that of regular frame structures. Understanding the nonlinear response of such structures is essential for evaluating their seismic performance and identifying potential weaknesses.

Therefore, there is a need to perform nonlinear seismic performance evaluation using pushover analysis to assess the behavior of different reinforced concrete building configurations and compare their strength, ductility, displacement capacity, and damage patterns under earthquake loading.

1.3 Objectives

The main objectives of the present study are:

1. To perform a nonlinear static pushover analysis of reinforced concrete buildings using SAP2000.
2. To evaluate the seismic performance of different structural configurations, including regular frame buildings, irregular setback buildings, core shear wall buildings, and perimeter shear wall buildings.
3. To compare the capacity curves, performance points, and displacement capacities of different building models.
4. To study the formation and distribution of plastic hinges under seismic loading.
5. To evaluate the influence of structural irregularity and shear wall systems on seismic behavior.
6. To assess the strength, stiffness, ductility, and overall performance of various building configurations (Regular G+15 & G+20 building, irregular G+20 building, irregular G+20 with shear wall core, and irregular G+20 with perimeter shear wall).
7. To identify the most effective structural system for improving seismic resistance.

1.4 Scope of Study

The scope of the present work is limited to the nonlinear seismic performance evaluation of reinforced concrete buildings through pushover analysis. The study has been carried out using SAP2000 software and includes the following aspects:

- Reinforced concrete building models only.
- One regular G+15 building model.
- One regular G+20 building model.
- One G+20 setback building model.
- One G+20 shear wall core building model.
- One G+20 perimeter shear wall building model.
- Linear modal analysis and response spectrum analysis.
- Nonlinear static pushover analysis in both X and Y directions.
- Uniform, IS 1893-consistent parabolic distribution (parabolic), and modal lateral load patterns.
- ATC-40 Capacity Spectrum Method for the determination of performance points.
- ASCE-based plastic hinge properties for beams and columns.
- Evaluation of capacity curves, hinge formation, displacement capacity, and structural performance.

The study does not include nonlinear time-history analysis, soil-structure interaction effects, foundation flexibility, material deterioration, or construction-related uncertainties.

1.5 Organization of Report

The report is organized into seven chapters to systematically present the methodology, analysis, results, and conclusions of the study.

Chapter 1 – Introduction presents the background, problem statement, objectives, scope, and organization of the study.

Chapter 2 – Literature Review summarizes previous research related to seismic performance evaluation, pushover analysis, structural irregularities, and shear wall systems.

Chapter 3 – Methodology describes the modeling procedure, software used, design codes, building configurations, loading conditions, hinge properties, and pushover analysis methodology adopted in the study.

Chapter 4 – Linear Analysis Results presents the results obtained from modal analysis and response spectrum analysis, including natural periods, mode shapes, and seismic response parameters.

Chapter 5 – Nonlinear Analysis Results discusses the pushover analysis results, including capacity curves, performance points, hinge formation patterns, and comparison of seismic behavior among different building models.

Chapter 6 – Advanced Evaluation includes ductility assessment, overstrength evaluation, moment-curvature studies of representative beam and column sections, and performance-based assessment of the building models.

Chapter 7 – Conclusions and Future Scope summarizes the major findings of the study and provides recommendations for future research in the field of nonlinear seismic performance evaluation.

The report concludes with references and appendices containing supplementary calculations, SAP2000 output data, and additional figures used in the analysis.

CHAPTER 2
LITERATURE REVIEW

2.1 Introduction

The seismic performance of reinforced concrete structures has been a major area of research in structural engineering due to the increasing frequency of earthquake-induced damage worldwide. Traditional design approaches based on linear elastic analysis provide an estimate of structural demand but are unable to accurately represent the nonlinear behavior exhibited by structures during strong ground motion.

To overcome these limitations, researchers have extensively investigated nonlinear analysis techniques such as pushover analysis, nonlinear time-history analysis, and performance-based seismic design. Among these methods, pushover analysis has emerged as a practical and efficient tool for evaluating structural capacity, identifying plastic hinge formation, estimating performance points, and understanding collapse mechanisms.

Numerous studies have been conducted to investigate the seismic behavior of regular and irregular buildings, the effectiveness of shear wall systems, and the influence of structural configuration on overall performance. This chapter reviews previous research related to nonlinear seismic evaluation, structural irregularity, and shear wall systems, providing the foundation for the present study.

2.2 Previous Research

1. Avanapu Sri Hari and B. Prudvi Rani (2025)

Citation

Hari, A. S., and B. P. Rani, “Seismic Performance of RC Framed Structures with Vertical Single Setback Irregularity,” *International Journal for Research in Applied Science & Engineering Technology (IJRASET)*, vol. 13, no. 11, Nov. 2025.

Review

Avanapu Sri Hari and B. Prudvi Rani (2025) investigated the seismic behavior of RC framed buildings with single vertical setback irregularity using response spectrum analysis in ETABS. The study found that setback irregularity significantly increases lateral displacement and storey drift near the setback level and causes non-uniform base shear distribution. The authors concluded that vertical setbacks adversely affect seismic performance and require special consideration in design.

2. Pradhumn Agrawal and Goutam Ghosh (2025)

Citation

Agrawal, P., and G. Ghosh, “Seismic Performance of Step-back and Set-back Building Resting on Hill-Slope,” *Procedia Structural Integrity*, vol. 70, pp. 113–120, 2025. DOI: 10.1016/j.prostr.2025.07.033.

Review

Agrawal and Ghosh (2025) studied step-back and setback buildings on hill slopes, considering soil-structure interaction effects. Their results showed that setback buildings exhibited lower displacement and base shear compared to step-back configurations. The study highlighted the importance of soil flexibility and building geometry in seismic performance assessment.

3. Mehran Aslani and Payam Tehrani (2025)

Citation

Aslani, M., and P. Tehrani, “Seismic Response and Collapse Capacity Assessment of Dual RC Buildings with Vertical Irregularities in Shear Walls,” *Scientific Reports*, vol. 15, 2025, Article 9966.

Review

Aslani and Tehrani (2025) evaluated RC dual systems with vertical irregularities in shear wall height using nonlinear dynamic analysis and fragility assessment. The study reported that irregularities occurring at lower levels significantly increased structural response and collapse probability, while upper-level irregularities had comparatively minor effects. The authors proposed a new irregularity index to improve seismic code provisions.

4. Ankan Barua, Sohel Rana, A.H.M. Shahidul Islam, and Shafayat Bin Ali (2026)

Citation

Barua, A., S. Rana, A. H. M. S. Islam, and S. B. Ali, “Seismic Response Assessment of RC Frame-Shear Wall Buildings with Vertical Setback Irregularities,” *Proceedings of the 8th International Conference on Civil Engineering for Sustainable Development (ICCESD 2026)*, Bangladesh, 2026.

Review

Barua et al. (2026) assessed RC frame-shear wall buildings with vertical setback irregularities using nonlinear time history and pushover analyses. Their findings indicated that setback irregularities increase higher mode effects, amplify peak floor acceleration, and reduce structural capacity. The study emphasized that multiple setbacks adversely affect seismic resistance.

5. Pranab Kumar Das and Mainak Mallik (2025)

Citation

Das, P. K., and M. Mallik, “Seismic Response of Setback Building in Hilly Region with Effect of Lift Well,” *Materials Research Proceedings*, vol. 48, pp. 225–233, 2025. DOI: 10.21741/9781644903414-25.

Review

Das and Mallik (2025) investigated setback buildings in hilly regions with and without lift wells acting as shear walls. The study showed that incorporating lift wells improved stability, reduced stress concentration, and enhanced seismic performance. The results demonstrated the effectiveness of shear wall-like elements in irregular buildings

2.3 Research Gap

A considerable amount of research has been conducted on the nonlinear seismic behavior of reinforced concrete buildings, including studies on regular frames, vertically irregular structures, and shear wall systems. However, most published investigations evaluate these structural configurations independently and under different modeling assumptions, making direct comparison difficult. Furthermore, relatively few studies have performed a comprehensive comparative pushover assessment of regular, setback, core shear wall, and perimeter shear wall buildings using a consistent modeling framework based on Indian seismic design provisions.

The literature indicates a need for comparative evaluation of different structural systems subjected to identical loading conditions, material properties, seismic parameters, and performance assessment procedures. In particular, studies integrating IS 1893:2016 seismic provisions with ATC-40 performance evaluation and FEMA/ASCE hinge modeling remain limited. The present work addresses this gap by conducting a unified nonlinear seismic assessment of five reinforced concrete building configurations and comparing their strength, stiffness, ductility, overstrength, hinge formation characteristics, and overall seismic performance.

2.4 Need for the Present Study

The present study aims to evaluate the nonlinear seismic behavior of five reinforced concrete building models, namely G+15 regular frame, G+20 regular frame, G+20 setback irregular frame, G+20 core shear wall frame, and G+20 perimeter shear wall frame, using pushover analysis in SAP2000. The study seeks to compare capacity curves, performance points, hinge formation mechanisms, displacement capacity, and overall seismic performance in order to identify the most effective structural configuration for earthquake-resistant design.

CHAPTER 3
METHODOLOGY

3.1 Research Flowchart

The overall methodology adopted in this study is illustrated in Figure 3. The study begins with the development of five reinforced concrete building models in SAP2000. Linear static and dynamic analyses are first performed to evaluate the elastic behavior of the structures. Modal analysis is then conducted to obtain the fundamental periods and mode shapes. Response Spectrum Analysis (RSA) is carried out according to the IS 1893 provisions. Subsequently, a nonlinear static pushover analysis is performed using predefined hinge properties. The performance point of each structure is determined using the ATC-40 Capacity Spectrum Method. Finally, the seismic performance of all building models is compared based on capacity curves, performance points, displacement capacity, base shear capacity, and hinge formation patterns.

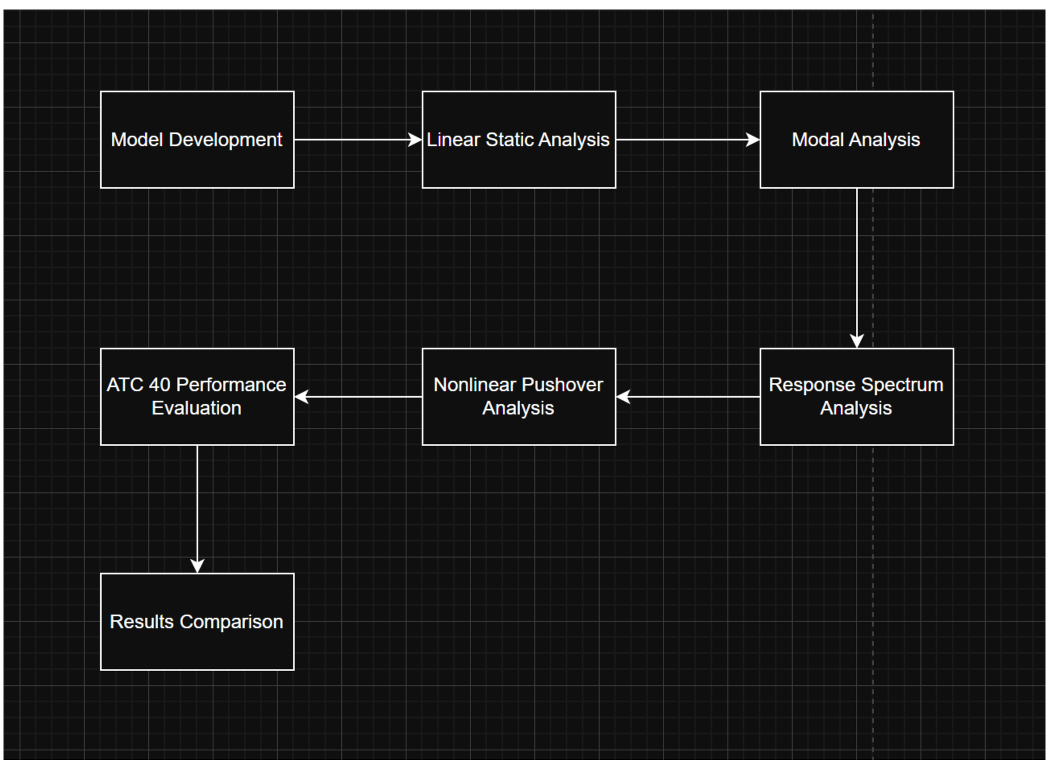

Fig. 3: Research Flowchart

3.2 Software Used

The structural modelling and analysis were performed using **SAP2000**, a finite element-based structural analysis software developed by Computers and Structures Inc. (CSI). SAP2000 provides advanced capabilities for linear and nonlinear analysis of structures and is widely used for seismic performance evaluation of reinforced concrete buildings.

The software was utilized for:

- Structural modelling
- Load assignment
- Modal analysis
- Response Spectrum Analysis
- Nonlinear hinge assignment
- Pushover analysis
- Capacity spectrum generation
- Performance point determination

3.3 Design Codes and Guidelines

The analysis and design procedures adopted in this study are based on the following codes and guidelines:

Code/Guideline	Description
IS 456:2000	Plain and Reinforced Concrete – Code of Practice
IS 1893 (Part 1): 2016	Criteria for Earthquake-Resistant Design of Structures
ATC-40	Seismic Evaluation and Retrofit of Concrete Buildings
FEMA 356	Prestandard and Commentary for Seismic Rehabilitation of Buildings
ASCE 41-17	Seismic Evaluation and Retrofit of Existing Buildings

These provisions were used for determining seismic loads, hinge properties, and performance levels.

3.4 Building Models

Five reinforced concrete building models were developed to investigate the influence of building height, vertical irregularity, and shear wall configuration on seismic performance.

Model 1: G+15 Regular RC Frame

This model consists of a regular reinforced concrete moment-resisting frame with fifteen stories above ground level. The building has uniform geometry and stiffness distribution throughout its height.

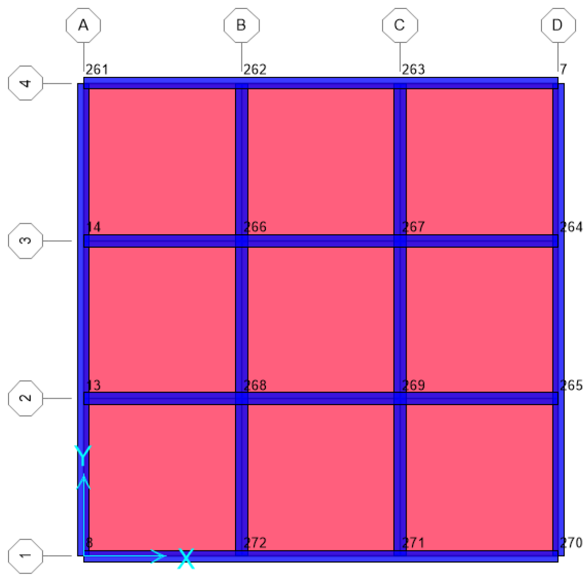

Fig. 4: Plan view for G+15 model

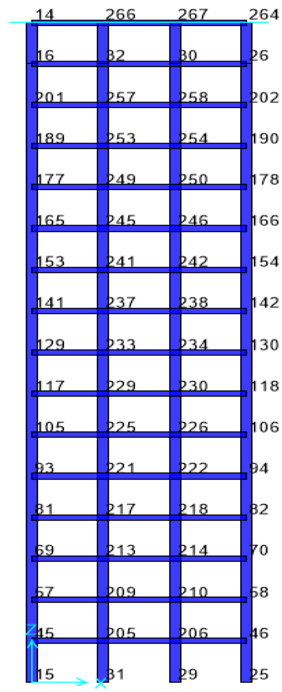

Fig. 5: Elevation View of G+15 model

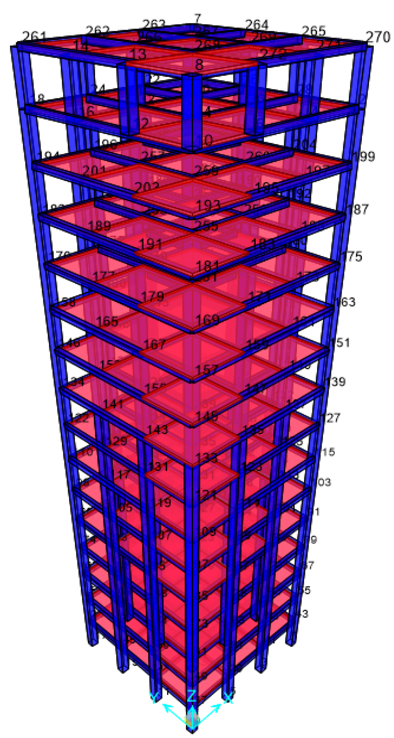

Fig. 6: 3D View of G+15 model

Model 2: G+20 Regular RC Frame

This model consists of a twenty-story regular reinforced concrete frame building without any geometric irregularities or shear walls.

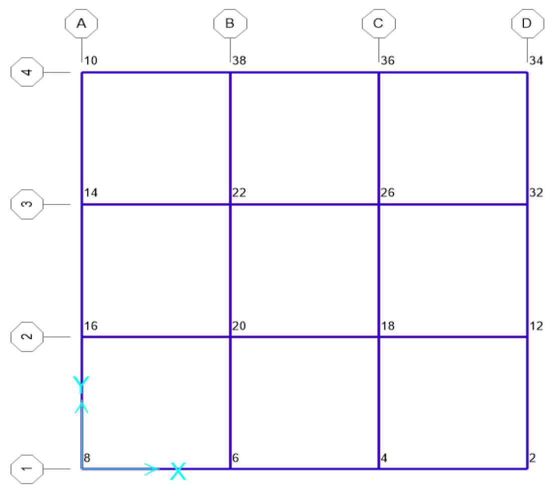

Fig. 7: Plan View of G+20 Regular Model

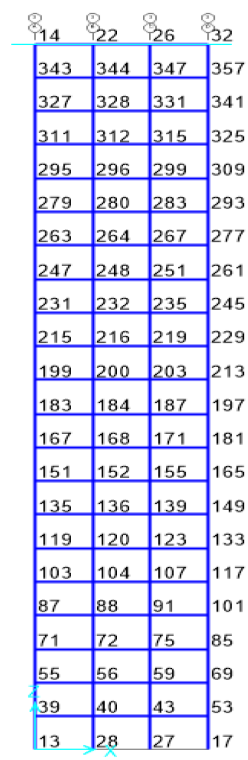

Fig. 8: Elevation view of G+20 regular model

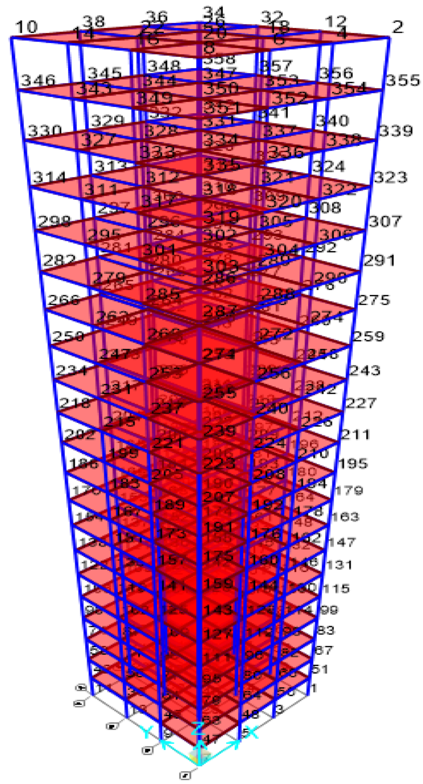

Fig. 9: 3D View of G+20 Regular model

Model 3: G+20 Setback Irregular Building

This model incorporates vertical geometric irregularity in the form of setbacks at upper stories. The setback configuration introduces discontinuity in mass and stiffness distribution along the building height.

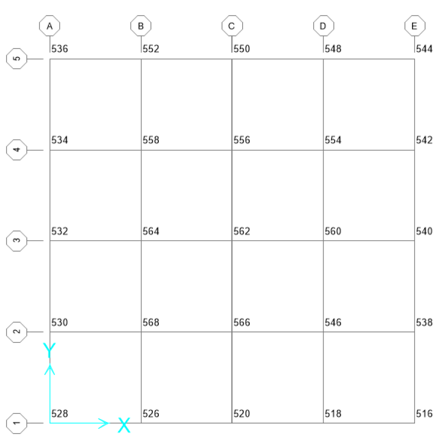

Fig. 10: Plan View of G+20 Setback Irregular Model

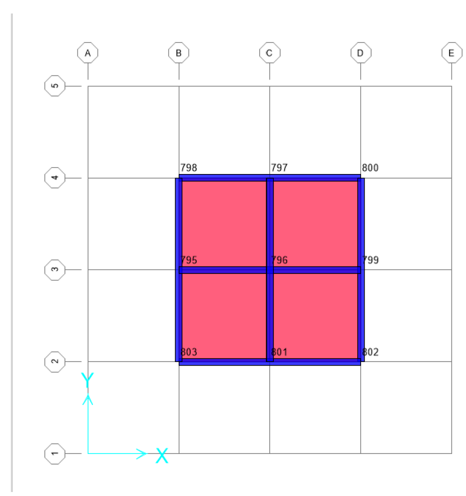

Fig. 11: Setback Plan View of G+20 Setback Irregular Model

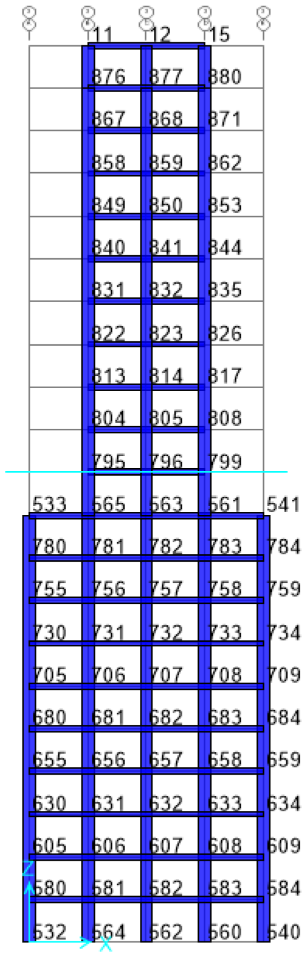

Fig. 12: Elevation View of G+20 Setback Irregular Model

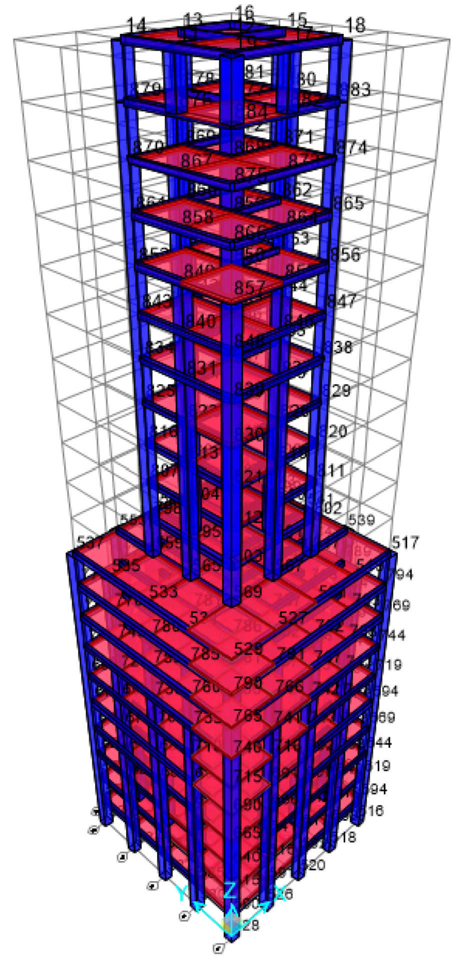

Fig. 13: 3D view of G+20 Setback Irregular Model

Model 4: G+20 Core Shear Wall Building

This model includes reinforced concrete shear walls located around the central core region. The shear walls provide additional lateral stiffness and improve seismic resistance.

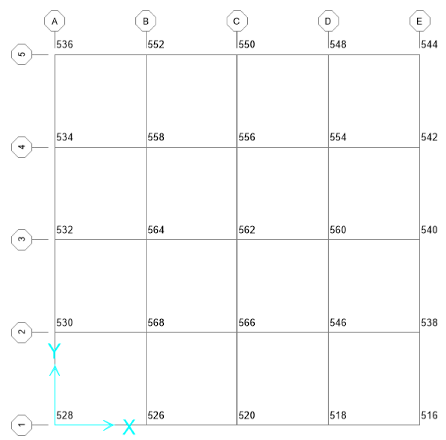

Fig. 14: Plan View of G+20 Core Shear Wall Model

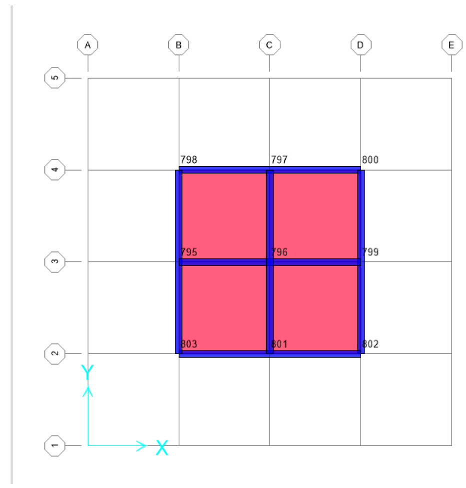

Fig. 15: Setback Plan View of G+20 Core Shear Wall Model

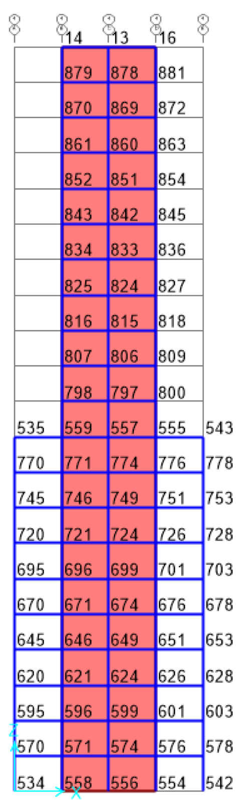

Fig. 16: Elevation View of G+20 Core Shear Wall Model

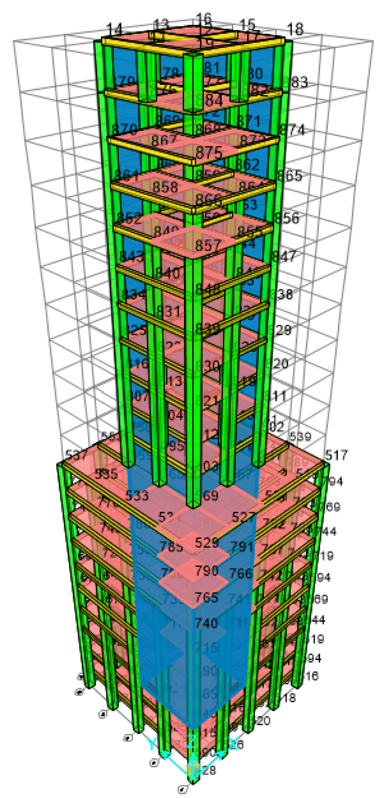

Fig. 17: 3D View of G+20 Core Shear Wall Model

Model 5: G+20 Perimeter Shear Wall Building

This model consists of reinforced concrete shear walls positioned along the perimeter of the structure. The perimeter wall arrangement increases lateral stiffness and enhances resistance against earthquake forces.

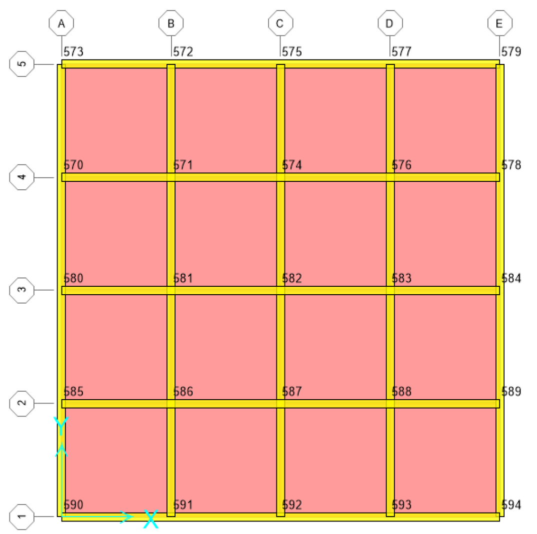

Fig. 18: Plan view of G+20 Perimeter shear wall model

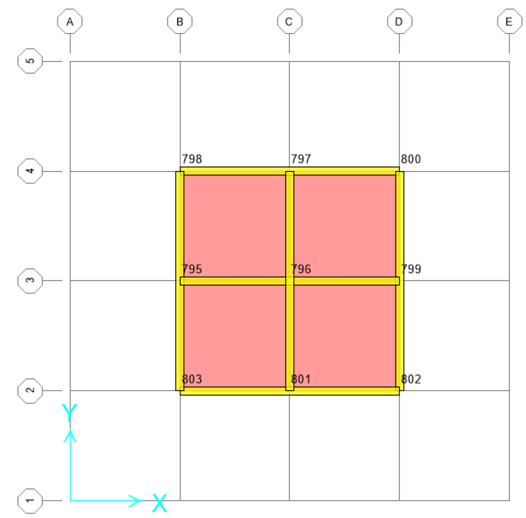

Fig. 19: Plan view of G+20 Perimeter shear wall model at setback

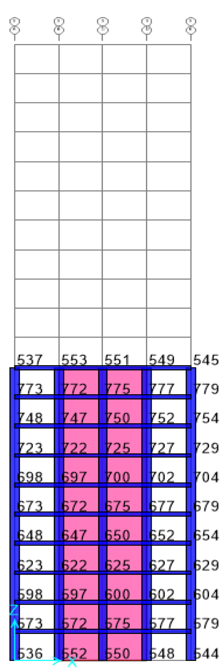

Fig. 20: Elevation View with shear walls till setback

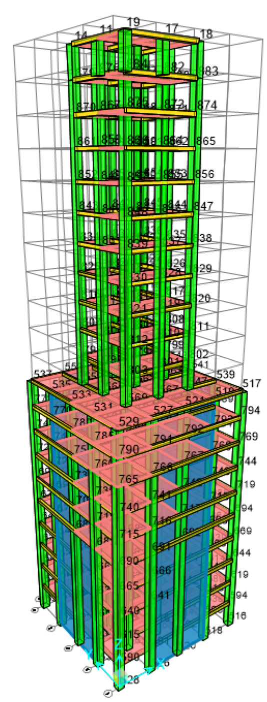

Fig. 21: 3D View with perimeter shear walls.

Table 3.1: Modeling Assumptions Adopted in the Present Study

Assumption	Considered / Neglected	Rationale
Material nonlinearity	Considered	Captured through FEMA/ASCE hinge properties during pushover analysis
Geometric nonlinearity (P-Delta)	Considered	To account for second-order effects under lateral loading
Soil-structure interaction	Neglected	Fixed-base condition assumed for simplicity and consistency among models
Foundation flexibility	Neglected	Supports are modeled as fixed restraints
Masonry infill walls	Neglected	Only the primary RC structural system is considered
Torsional irregularity	Not explicitly introduced	Building layouts are maintained symmetrically in plan
Shear wall material nonlinearity	Not modeled through the wall hinges	Walls modeled as elastic shell elements providing lateral stiffness
Damping	5% critical damping	As recommended by IS 1893 for RC structures
Earthquake loading	Response Spectrum and Pushover	To evaluate both elastic and inelastic seismic response
Hinge modeling	FEMA/ASCE default hinges	Beam M3 and Column PMM hinges are assigned automatically in SAP2000

3.5 Material Properties

The material properties used in all structural models are summarized in Table 3.1.

Table 3.2 Material Properties

Property	Value
Concrete Grade for columns	M35
Concrete Grade for beams	M30
Modulus of Elasticity	27.39 GPa
Poisson's Ratio	0.20
Density of Concrete	25 kN/m^3
Steel Grade	Fe415
Yield Strength of Steel	415 MPa
Modulus of Elasticity of Steel	200 GPa

3.6 Loading Details

The structural models were subjected to dead load, live load, and seismic load in accordance with IS 875 and IS 1893 provisions.

Dead Load

Dead loads include the self-weight of structural members, floor finishes, wall loads, and other permanent loads.

Live Load

Live loads were assigned according to the occupancy requirements specified in IS 875 (Part 2).

Seismic Load

Earthquake loads were applied using Response Spectrum Analysis based on IS 1893 (Part 1): 2016. The seismic parameters considered include:

- Seismic Zone III
- Seismic Zone Factor (Z) = 0.16
- Importance Factor (I) = 1
- Response Reduction Factor (R) = 5
- Soil Type = Medium Soil (Type 2)
- Damping Ratio = 5%

3.7 Hinge Properties

To simulate nonlinear structural behavior during pushover analysis, plastic hinges were assigned at critical locations of beams and columns.

Beam Hinges

Moment hinges (M3) were assigned at both ends of beam elements. These hinges represent flexural yielding behavior under increasing lateral loads.

Location: 0.05L and 0.95L

Behaviour: Flexural yielding

Column Hinges

Axial force–biaxial moment interaction hinges (PMM) were assigned at both ends of column elements. These hinges capture the combined effects of axial force and bending moments.

Location: 0.05L and 0.95L

Behaviour: Axial force–biaxial moment interaction

The hinge properties were generated automatically in SAP2000 according to the recommendations of **ASCE 41-17**.

Linear Analysis, Modal Analysis, Response Spectrum Analysis, and Nonlinear Pushover Analysis were performed on every five models.

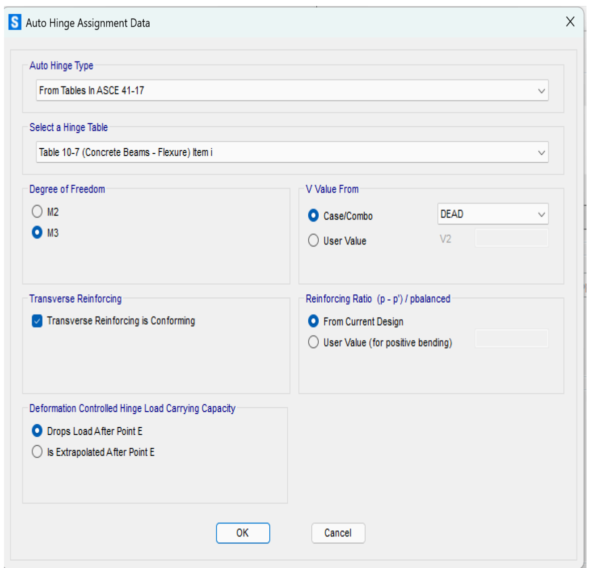

Fig. 22: Hinge Assignment of Beams

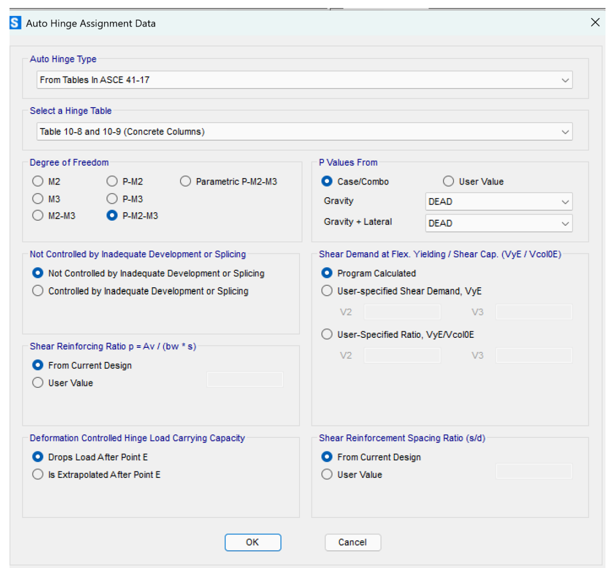

Fig. 23: Hinge Assignment of Columns

3.8 Pushover Load Cases

Six pushover load cases were defined to evaluate structural performance under different lateral load distributions.

Table 3.3 Pushover Load Cases

Load Case	Description
PUSHX_Parabolic	Parabolic Load Pattern in X Direction
PUSHY_Parabolic	Parabolic Load Pattern in Y Direction
PUSHX_UNI	Uniform Load Pattern in X Direction
PUSHY_UNI	Uniform Load Pattern in Y Direction
PUSHX_MODAL	Modal Load Pattern in X Direction
PUSHY_MODAL	Modal Load Pattern in Y Direction

The different loading patterns were used to evaluate the sensitivity of structural response to lateral force distribution.

3.8.1 Selection of Target Displacement

In nonlinear static pushover analysis, a target displacement is specified to represent the expected maximum deformation demand that may occur during severe seismic loading. In the present study, the target displacement was initially selected as 4% of the total building height, which is consistent with deformation limits commonly adopted in performance-based seismic evaluation procedures such as FEMA 356 and the ATC-40 Capacity Spectrum Method.

The selected target displacement was intended to ensure that sufficient nonlinear behavior, hinge formation, stiffness degradation, and damage progression could be captured during the analysis. The displacement-controlled pushover procedure was therefore allowed to continue until either the target displacement was reached or the structure became unable to sustain additional lateral loading.

However, several building models did not reach the prescribed target displacement. In such cases, the analysis terminated earlier due to numerical convergence difficulties, excessive hinge formation, local instability, or attainment of the maximum number of allowable null steps. Therefore, the final displacement achieved by each model was taken as the last converged displacement and was used for subsequent evaluation of structural capacity and seismic performance.

The comparison between the specified target displacement and the maximum achieved displacement is presented in Table 3.3.

Table 3.4: Target vs. Achieved Displacements.

Model	Building Height (m)	Target Displacement	Max Achieved Displacement	Percentage Achieved (%)
G+15	48	1.92 m	0.7078 m	36.86
G+20	63	2.52 m	1.0080 m	40.00
G+20 Irregular	63	2.52 m	1.9265 m	76.44
G+20 CSW	63	2.52 m	0.1660 m	6.587
G+20 PSW	63	2.52 m	0.7745 m	30.73

Where, Percentage Achieved = (Target/Achieved)*100

Although a target displacement equal to 4% of the building height was specified, several models terminated at lower displacement levels due to convergence limitations and progressive nonlinear behavior. Consequently, the last converged displacement was considered as the ultimate displacement for performance evaluation.

3.9 ATC-40 Procedure

The seismic performance of all models was evaluated using the Capacity Spectrum Method recommended by ATC-40.

The procedure involves converting the pushover curve into spectral acceleration and spectral displacement coordinates. The intersection of the structural capacity curve and the demand spectrum defines the performance point of the building.

The performance point represents the expected displacement demand during the design earthquake and is used to assess the performance level of the structure.

The performance levels considered include:

- Immediate Occupancy (IO)
- Life Safety (LS)
- Collapse Prevention (CP)

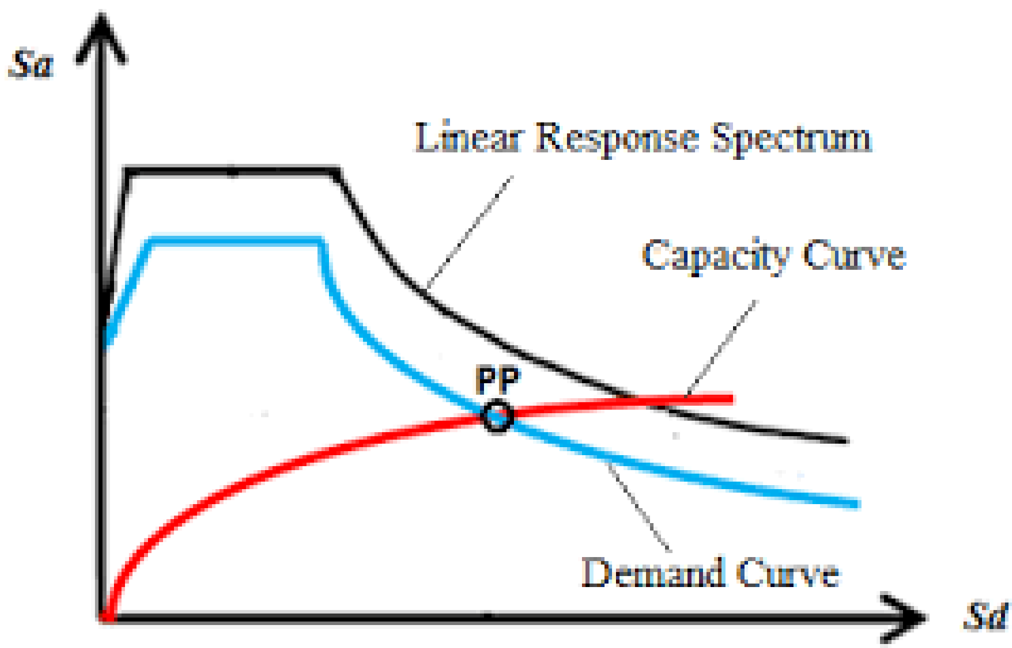

Fig. 24: Typical Performance Point Diagram.

3.10 Geometric Configuration of Models

Table 3.5 Geometric Parameters of Building Models

Parameter	Value
Number of Bays (X)	4
Number of Bays (Y)	4
Bay Width	4 m
Storey Height	3 m
Ground Storey Height	3 m
Total Plan Dimension for G+15 & G+20	12m x 12 m
Total regular plan dimension for all G+20 setback models	16m x 16m
Total setback plan Dimension for all G+20 setback models	8m x 8m
G+15 Building Height	48 m
G+20 Building Height	63 m
Slab Thickness	150 mm
Beam Size	300x400 mm
Column Size	800x800 mm
Shear Wall Thickness	250 mm

3.11 Vertical Geometric Irregularity Verification

IS 1893:2016 Requirement

According to IS 1893 (Part 1): 2016, Table 6, a building is considered vertically geometrically irregular if the horizontal dimension of the lateral force-resisting system in any storey exceeds **150% of that in an adjacent storey**.

Mathematically: $L_1/L_2 > 1.5$

Where, L_1 = larger plan dimension
L_2 = smaller adjacent plan dimension

Setback Building Verification

For the present G+20 setback structure:

Level	Plan Dimension (m)
Ground to 10th Floor	16 × 16
11th Floor to Roof	8 × 8

Therefore, the dimension ratio = 16/8 = 2.
Since 2 > 1.5, the structure satisfies the criteria for **Vertical Geometric Irregularity** as specified in IS 1893:2016 Table 6.

Table 3.6: Irregularity Check

Parameter	Value
Lower storey dimension	16 x 16 m
Upper storey dimension	8 x 8 m
Dimension Ratio	2
IS 1893 Limit	> 1.5
Status	The building is irregular

Numerical Convergence Considerations

The nonlinear pushover analyses were performed using displacement-controlled loading in SAP2000. Automatic step increment procedures were adopted to ensure solution stability during hinge formation and stiffness degradation. For certain models, particularly the setback and shear wall configurations, the analysis terminated prior to reaching the specified target displacement due to convergence difficulties and the occurrence of null-step iterations. Such behavior is commonly observed in nonlinear static analysis when rapid stiffness changes occur following hinge formation.

Despite these numerical limitations, all analyses successfully progressed beyond their respective performance points, enabling reliable assessment of structural capacity, hinge formation patterns, and seismic performance levels.

Chapter 4
Linear Analysis Results

4.1 Introduction

The nonlinear seismic evaluation carried out in the present study is based on the structural characteristics obtained from linear analysis. Therefore, before performing pushover analysis, each building model was evaluated using modal analysis and response spectrum analysis in accordance with IS 1893 (Part 1): 2016.

The results obtained from the linear analysis provide important information regarding the dynamic properties, stiffness characteristics, and seismic force demands of the structures. These results serve as the basis for defining the pushover loading patterns and for interpreting the nonlinear behaviour observed during subsequent analysis.

This chapter presents the modal properties and response spectrum results of all building models and establishes the relationship between linear and nonlinear seismic performance.

4.2 Modal Analysis Results

Purpose

This section answers: Which building is stiffer? Which building is more flexible? How did irregularity and shear walls affect dynamic behaviour?

Table 4.1 Fundamental Time Periods

Model	Tx (sec)
G+15 Regular	2.031
G+20 Regular	2.837
G+20 Setback	2.071
G+20 Core Wall	1.32
G+20 Perimeter Wall	1.602

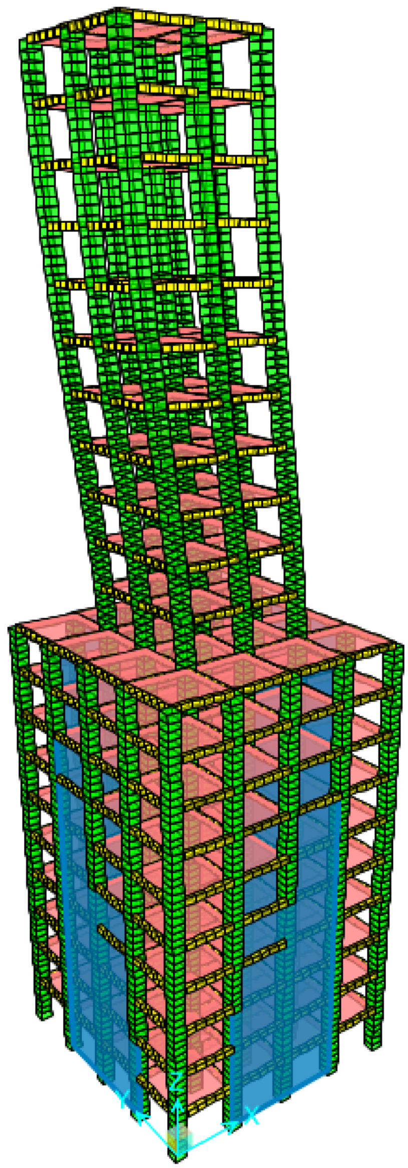

Fig. 25: Mode 1 Shape of Model 5

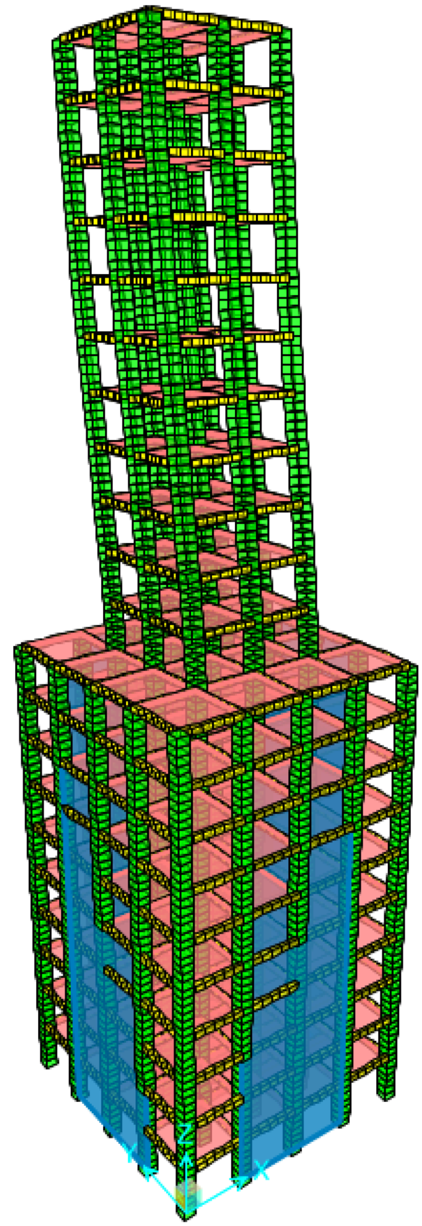

Fig. 26: Mode 2 Shape of Model 5

Discussion

The fundamental time period increased with an increase in building height due to a reduction in overall lateral stiffness. Consequently, the G+20 regular building exhibited a higher natural period than the G+15 building.

The introduction of geometric irregularity through setback modification altered the distribution of mass and stiffness, resulting in a change in modal characteristics compared to the regular configuration.

The core shear wall and perimeter shear wall models exhibited significantly lower natural periods owing to the substantial increase in lateral stiffness provided by the shear wall systems. Among all models, the perimeter shear wall configuration demonstrated the greatest stiffness, resulting in the lowest fundamental time period.

These observations indicate that the inclusion of shear walls effectively controls lateral deformation and enhances seismic resistance.

The modal analysis results obtained in Project 1 were subsequently used in Project 2 for the development of modal pushover load patterns. The dominant mode shapes identified from the modal analysis were converted into equivalent lateral force distributions for nonlinear static analysis.

4.3 Response Spectrum Analysis Results

Purpose

This section answers: How much seismic force does each building attract?

Before pushover, we need to know that.

Table 4.2 Response Spectrum Base Shear

Model	Max RSA Base Shear X (kN)
G+15 Regular	326.292
G+20 Regular	452.75
G+20 Setback	538
G+20 Core Wall	1035.83
G+20 Perimeter Wall	1501

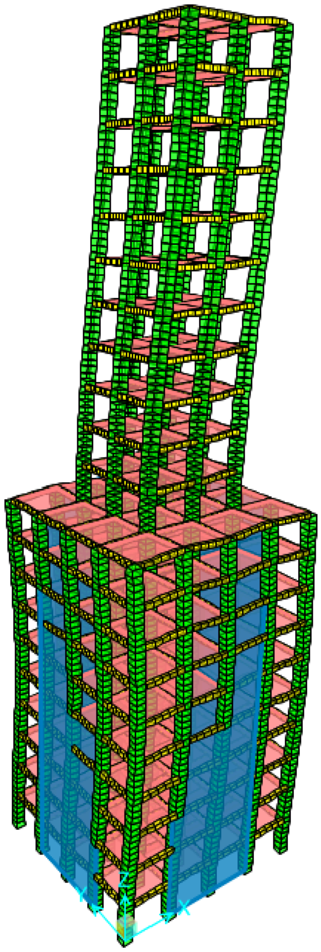

Fig. 27 Typical Deformation of Model 5 under RSX Loading.

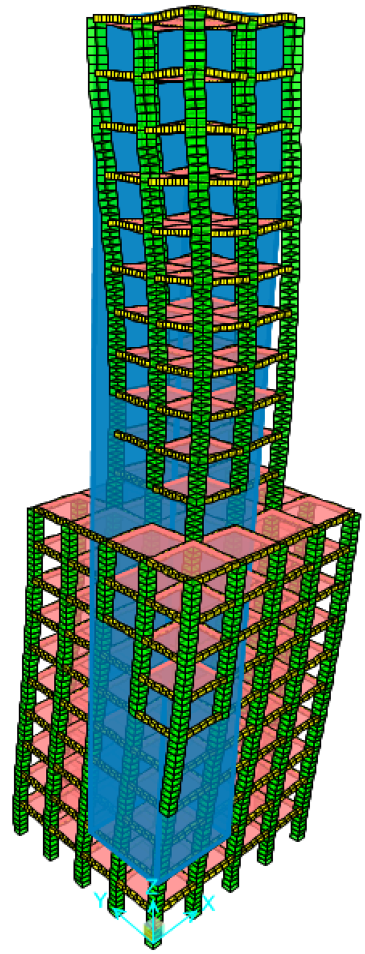

Fig. 28: Typical Deformation of Model 4 under RSX Loading.

Discussion

The response spectrum analysis results indicate that the seismic force demand varies significantly with structural configuration. Buildings possessing greater lateral stiffness attract larger base shear forces due to their lower fundamental periods.

The shear wall models exhibited higher base shear values compared to the corresponding moment-resisting frame structures. This behaviour is attributed to the increased stiffness of the shear wall systems, which results in greater acceleration demand during seismic excitation.

The setback building demonstrated a modified force distribution due to the discontinuity in stiffness and mass above the setback level. The redistribution of seismic forces observed in the response spectrum analysis provides an indication of the potential concentration of damage in the irregular portions of the structure.

4.4 Link Between Linear and Nonlinear Analysis

The results obtained from modal analysis and response spectrum analysis were used as input for the nonlinear seismic evaluation. The dominant vibration modes determined from modal analysis were utilized to generate modal pushover load patterns, while the seismic force demand obtained from response spectrum analysis was used as a reference for evaluating the reserve strength and overstrength characteristics of the buildings.

By comparing the elastic response obtained from Project 1 with the nonlinear behaviour obtained in Project 2, a comprehensive assessment of structural performance under earthquake loading becomes possible. This comparison allows evaluation of stiffness degradation, ductility capacity, hinge formation sequence, and collapse resistance of different structural configurations.

Inter-storey drift evaluation was carried out in Project 1 using Response Spectrum Analysis in accordance with IS 1893:2016 Clause 7.11.1. The maximum permissible drift limit was 0.004h, corresponding to 12 mm for a typical storey height of 3 m. Detailed drift profiles and compliance verification for all structural models are presented in Project 1. Since the present study focuses on nonlinear seismic performance through pushover analysis, the drift results are not reproduced here.

Model	Max Drift (mm)	IS 1893 Limit (mm)	Status
G+15	1.412	12	Pass
G+20	1.4	12	Pass
G+20 Irregular	1.631	12	Pass
G+20 CSW	1.406	12	Pass
G+20 PSW	1.26	12	Pass

Chapter 5
Nonlinear Static (Pushover) Analysis Results

5.1 Introduction

This chapter presents the results obtained from the nonlinear static pushover analysis performed on all building models. The analysis was conducted using parabolic, uniform, and modal lateral load patterns in both principal directions. Capacity curves, performance points, and hinge formation characteristics are evaluated to assess the seismic performance of regular, irregular, and shear wall structures.

The results are compared to investigate the influence of building height, geometric irregularity, and shear wall systems on structural capacity, ductility, and damage distribution.

The respective loading patterns: parabolic, Modal, and Uniform were calculated based on the following procedure.

The lateral load was applied to the central joint of each storey, as a rigid diaphragm was assigned to each storey.
For regular buildings (Model 1 and Model 2), the lateral load was assigned to joint 266 under the monitored displacement of 4% of the building's total height in both x and y directions.
Monitored displacement = 4% of 63 m = 2.52 m displacement at the central joint in every storey.

For irregular building models (models 3, 4, and 5), the lateral loads were assigned to the central joint 12 under monitored displacement of 4% of the building's height in both x and y directions.
Monitored displacement = 4% of 63 m = 2.52 m displacement at the central joint in every storey.

Target displacement was specified as 4% of building height. However, nonlinear analysis terminated earlier in several models due to the formation of critical hinges and convergence limitations.

5.2 Capacity Curves

5.2.1 G+15 Regular Building

1. Uniform loading refers to the equivalent static method for distributing the same lateral earthquake forces at every storey = base shear/number of storeys.

2. Parabolic loading refers to the equivalent static method for distributing lateral earthquake forces along the height of a building, as per the IS 1893:2016 standard.

The lateral forces at every storey can be calculated by the given formula:

$$Q_i = V_B \left[\frac{W_i h_i^2}{\sum_{j=1}^{n} W_j h_j^2} \right]$$

where, Q_i = The lateral seismic force at any specific floor level (i)
V_B = Design Base Shear calculated for the structure.
W_i = Seismic weight of floor 'i.'
h_i = Height of floor 'i' from the base.
W_j = Seismic weight of floor 'j.'
h_j = Height of floor (j) from the base.
n = Number of storeys in the building.

3. To calculate the modal loading pattern (also known as the modal inertia load pattern) under the Dynamic Analysis / Response Spectrum Method of IS 1893:2016, the modal loading pattern depends on the specific mode shapes derived from dynamic eigenvalues.

   $Q_{ik} = V_B * [(W_i*\phi_{ik})/\sum W_i*\phi_{ik})$ where the lateral force Q_{ik} acting at floor level i for vibration mode k.
   $\varnothing_{ik}$ = Mode shape coefficient at floor i for mode k (derived from modal analysis).
   W_i = Seismic weight of floor i.
   V_B = Design base shear

1. Uniform loading pattern calculations:
   Uniform load (Q_i) = base shear/number of storeys
   Q_i = 238.172/21
   Therefore, Q_i = 11.34 kN each storey.

2. IS 1893-consistent parabolic distribution (parabolic):

parabolic load $Q_i = V_B \left[\frac{W_i h_i^2}{\sum_{j=1}^{n} W_j h_j^2} \right]$

Q_{21} = 238.172*(1521626/1E+07)

Q_{21} = 39.48 kN for the roof joint.

3. Modal loading pattern calculation:
   $Q_{21} = V_B * [(W_{21}*\phi_{21})/\sum W_{21}*\phi_{21})$
   = 238.172*[(7.59/80.98)]
   = 22.35 kN for the roof joint.

Likewise, the loads for every joint and every storey were calculated and applied as joint loads.

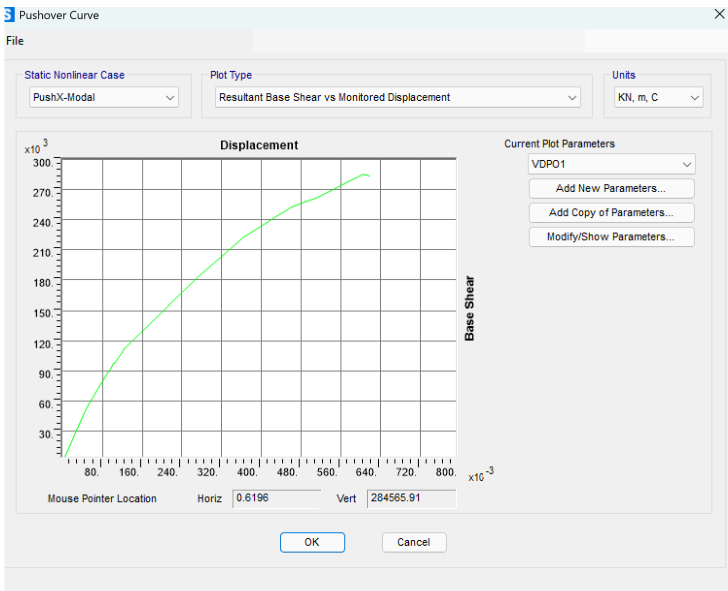

Fig. 29: PushX Modal Capacity Curve

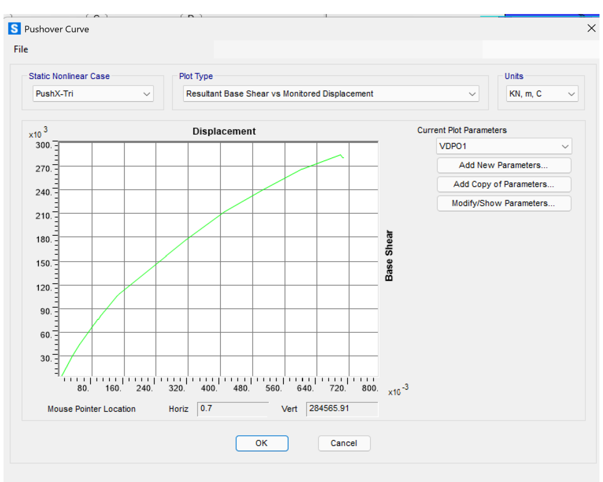

Fig. 30: PushX Parabolic Capacity Curve

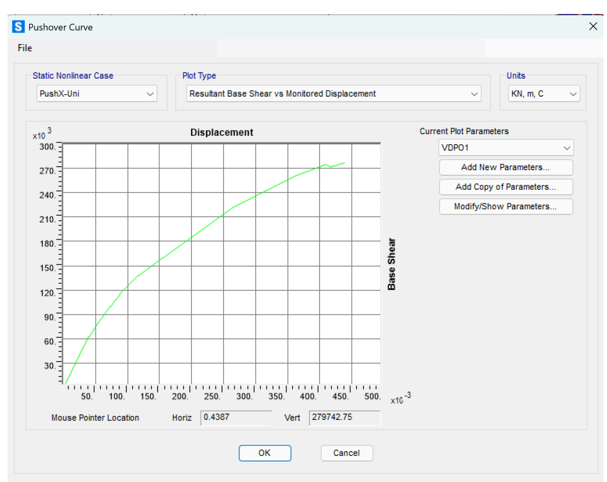

Fig. 31: PushX Uniform Capacity Curve

Discussion

The capacity curve of the G+15 regular frame building exhibits an initially steep linear region corresponding to elastic structural behavior. The first significant reduction in slope occurs following the formation of initial plastic hinges in the upper-storey beams, indicating the onset of stiffness degradation and redistribution of internal forces.

Beyond yielding, the structure continues to resist increasing lateral load, although with reduced stiffness. The absence of a pronounced strength plateau indicates that additional members progressively participate in resisting seismic demand, allowing the structure to develop reserve strength after initial yielding.

At the ATC-40 performance point, the building remains within the Immediate Occupancy (IO) performance level, suggesting that structural damage under the design earthquake is limited and substantial reserve capacity remains available before Life Safety (LS) or Collapse Prevention (CP) conditions are reached.

The regular configuration promotes a relatively uniform distribution of stiffness and mass along the height, resulting in gradual hinge development and stable nonlinear behavior.

Case	Peak Base Shear (kN)	Max Roof Disp. (m)	Performance Point Disp.	Performance Point Base Shear	First Hinge Step	First Hinge Location	First Hinge Member
X-Tri	284565.91	0.7078	0.027	25767.31	4th	various	beam
X-Uni	279742	0.4375	0.017	27120	2nd	various	beams
X-Modal	284565	0.619	0.023	26363	2nd	various	beams
Y-Tri	279742	0.707	0.027	25767	1st	5, 6, 7 storey	Beams
Y-Uni	274919	0.4387	0.017	27120	1st	4th storey	beams
Y-Modal	286495	0.6176	0.023	26363	1st	4th 5th storey	beams

Fig. 32: Load Pattern Results for G+15 Regular Building

5.2.2 G+20 Regular Building

1. Uniform loading pattern calculations:
   Uniform load (Q_i) = base shear/number of storeys
   $Q_i = 441.23/21$
   Therefore, $Q_i = 21.01$ kN for each storey.

2. parabolic loading pattern calculations:
   parabolic load
   $$Q_i = V_B \left[\frac{W_i h_i^2}{\sum_{j=1}^{n} W_j h_j^2} \right]$$
   $Q_{21} = 441.23*(5E+06/5E+07)$
   $Q_{21} = 44.29$ kN for the roof joint.

3. Modal loading pattern calculation:
   $Q_{21} = V_B * [(W_{21}*\phi_{21})/\sum W_{21}*\phi_{21})$
   = 441.23*[(17.95/364.54)]
   = 21.72 kN for the roof joint.

Likewise, the loads for every joint and every storey were calculated and applied as joint loads.

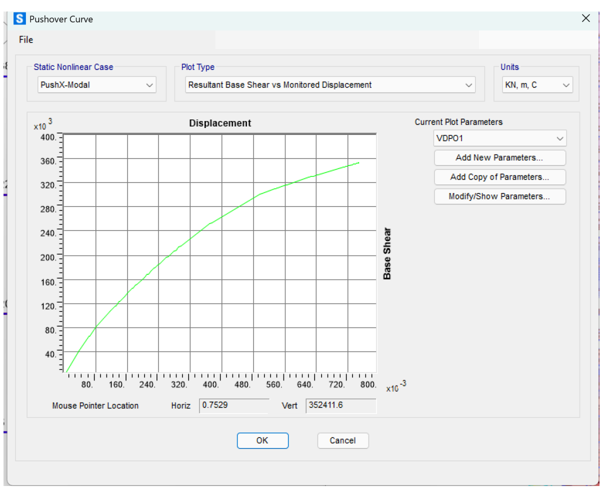

Fig. 33: PushX Modal

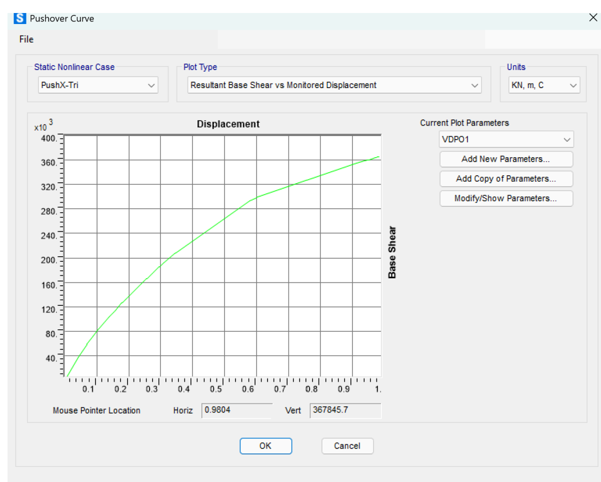

Fig. 34: PushX Parabolic

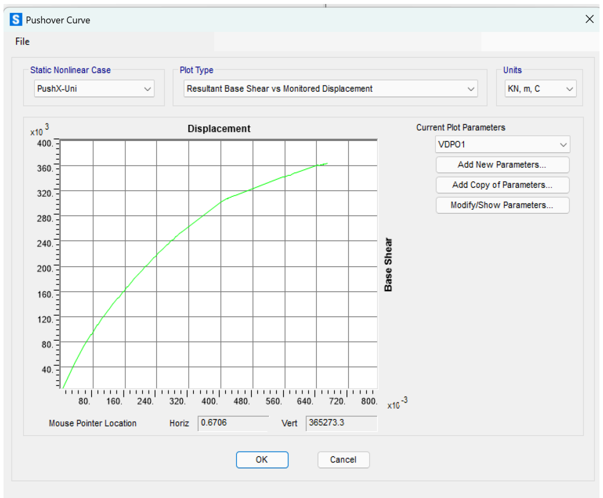

Fig. 35: PushX Uniform

Discussion

Compared to the G+15 structure, the G+20 regular frame exhibits a larger displacement demand due to its increased height and reduced overall lateral stiffness. The first significant slope change occurs at a lower effective stiffness level, indicating earlier participation of nonlinear deformation mechanisms.

Although the building experiences greater roof displacement, the capacity curve continues to increase without sudden strength degradation, demonstrating stable inelastic behavior. The larger deformation demand is primarily attributed to the longer fundamental period and greater flexibility associated with the increased height.

At the performance point, the structure remains within the Immediate Occupancy performance range. However, the increased displacement demand relative to the G+15 structure indicates a greater dependence on ductility to satisfy seismic performance requirements.

Case	Peak Base Shear (kN)	Max Roof Disp. (m)	Performance Point Disp.	Performance Point Base Shear	First Hinge Step	First Hinge Location	First Hinge Member
X-Tri	365273.3	0.9853	0.049	42858.704	2nd	various	beams
X-Uni	365273.3	0.6706	0.034	45826.826	1st step	5th & 6th	beams
X-Modal	352411	0.7529	0.041	44261.686	1st step	6th & 7th	beams
Y-Tri	370418	1.008	0.049	42858.704	2nd	various	beams
Y-Uni	361414.8	0.6373	0.034	45826.826	1st step	5th & 6th	beams
Y-Modal	365273.3	0.8456	0.041	44173.47	1st step	5th & 6th	beams

Fig. 36: Load Pattern Results for G+20 Regular Building

5.2.3 G+20 Setback Building

1. Uniform loading pattern calculations:
   Uniform load (Q_i) = base shear/number of storeys
   Q_i = 421.28/21
   Therefore, Q_i = 20.06 kN for each storey.

2. parabolic loading pattern calculations:
   parabolic load
   $$Q_i = V_B \left[\frac{W_i h_i^2}{\sum_{j=1}^{n} W_j h_j^2} \right]$$
   Q_{21} = 421.28*(2E+06/3E+07)
   Q_{21} = 32.25 kN for the roof joint.

3. Modal loading pattern calculation:
   $Q_{21} = V_B * [(W_{21}*\phi_{21})/\sum W_{21}*\phi_{21})$
   = 421.28*[(14.644/279.13)]
   = 22.1 kN for the roof joint.

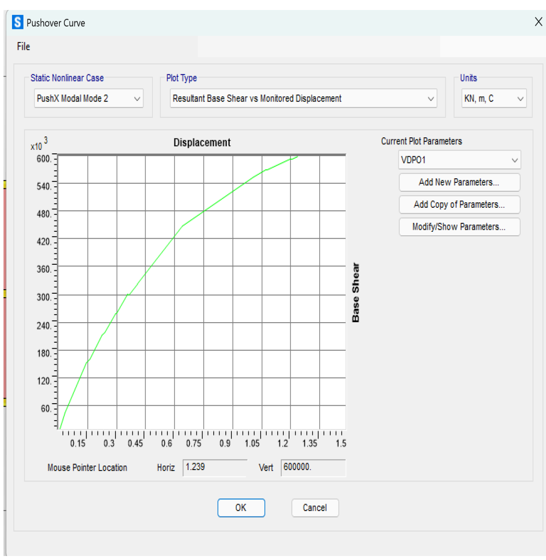

Fig. 37: PushX Modal

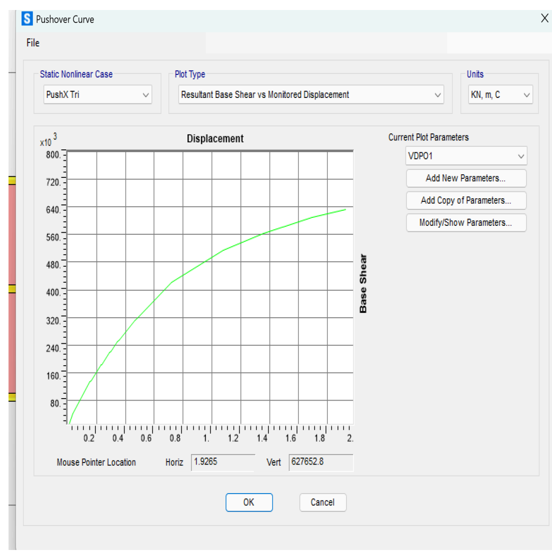

Fig. 38: PushX Parabolic

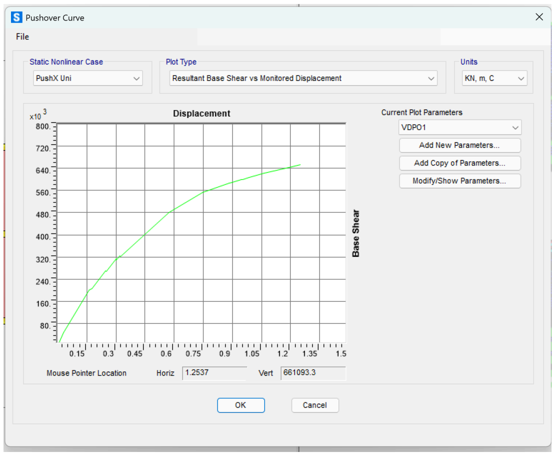

Fig. 39: PushX Uni

Discussion

The setback building exhibits a distinctly different capacity curve compared with the regular G+20 structure due to the presence of a major geometric discontinuity at the setback level. Although the structure maintains significant lateral strength, the displacement demand increases substantially because deformation becomes concentrated near the setback transition.

The reduction in plan dimension from 16 m × 16 m to 8 m × 8 m produces a dimension ratio of 2.0, exceeding the IS 1893:2016 threshold of 1.5 for vertical geometric irregularity. This abrupt change in stiffness causes a concentration of inter-storey drift and plastic hinge formation in the vicinity of the setback.

The increased displacement demand is not solely a consequence of reduced strength but is primarily caused by localized flexibility at the setback region. The setback effectively behaves as a deformation concentration zone, resulting in amplification of roof displacement even under moderate increases in base shear.

The hinge formation patterns observed during pushover analysis confirm this behavior, with initial yielding and subsequent damage concentrated at the tenth storey. This demonstrates that the irregularity governs the nonlinear response of the structure.

Potential measures for mitigating this behavior include the introduction of shear walls at the setback level, gradual tapering of the building geometry, or the incorporation of outrigger systems to improve force transfer across the discontinuity. Such measures would reduce drift concentration and improve overall seismic performance.

Case	Peak Base Shear (kN)	Max Roof Disp. (m)	Performance Point Disp.	Performance Point Base Shear	First Hinge Step	First Hinge Location	First Hinge Member
X-Tri	627652	1.9265	0.029	32912	2nd	various	beams
X-Uni	661093	1.2537	0.022	36289	2nd	various	beams
X-Modal	600000	1.239	0.025	34219	1st	10th storey	beams
Y-Tri	630225.1	1.9069	0.029	32912	1st	10th storey	beams
Y-Uni	653376	1.2022	0.022	36281	1st	10th storey	beams
Y-Modal	601929	1.2904	0.025	34212	1st	10th storey	beams

Fig. 40: Load Pattern Results for G+20 Irregular Building

5.2.4 G+20 Core Shear Wall Building

1. Uniform loading pattern calculations:
   Uniform load (Q_i) = base shear/number of storeys
   Q_i = 527/21
   Therefore, Q_i = 25.09 kN for each storey.

2. parabolic loading pattern calculations:
   parabolic load
   $$Q_i = V_B \left[\frac{W_i h_i^2}{\sum_{j=1}^{n} W_j h_j^2} \right]$$
   Q_{21} = 527*(25025671/47593656)
   Q_{21} = 277.1 kN for the roof joint.

3. Modal loading pattern calculation:
   $Q_{21} = V_B * [(W_{21}*\phi_{21})/\sum W_{21}*\phi_{21})$
   = 527*[(96.24/332.71)]
   = 152.44 kN for the roof joint.

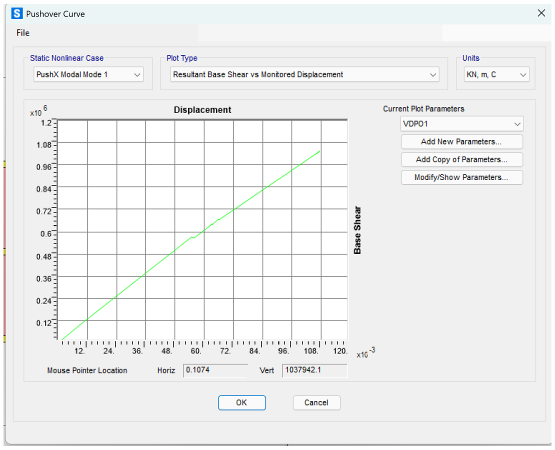

Fig. 41: PushX Modal

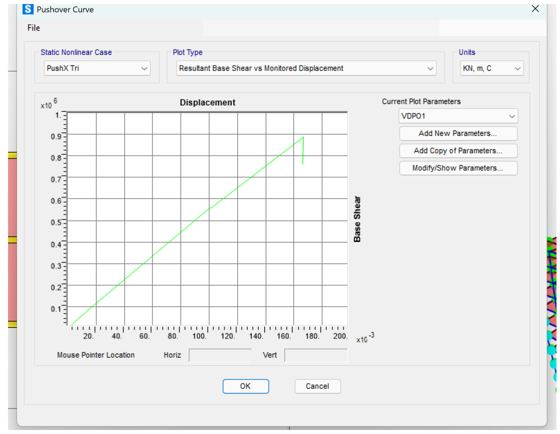

Fig. 42: PushX Parabolic

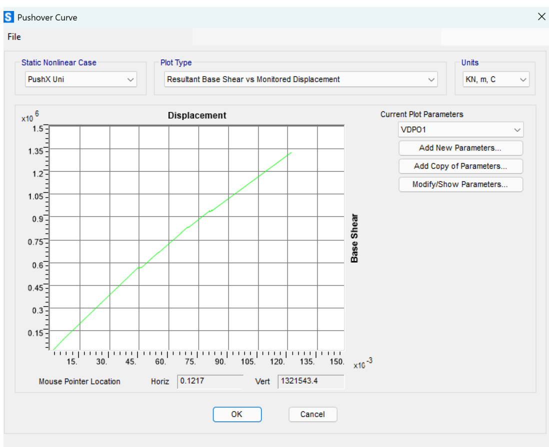

Fig. 43: PushX Uni

Discussion

The core shear wall model demonstrates the highest lateral stiffness among the investigated structures, resulting in the smallest performance point displacement and one of the highest lateral load capacities. The initial slope of the capacity curve is substantially steeper than that of the frame-dominated systems, indicating superior resistance to lateral deformation.

While increased stiffness improves drift control and strength, it does not necessarily imply superior ductility. The reduced deformation demand observed in the core wall structure is accompanied by lower displacement ductility compared with conventional frame systems. This illustrates a fundamental trade-off in seismic design: structures can achieve high strength through stiffness, high ductility through controlled inelastic deformation, or a balance of both.

The interaction between the moment-resisting frame and the core wall is a significant aspect of the structural response. As lateral loading increases, the wall resists a major portion of the overturning moment and lateral shear, thereby reducing demand on the surrounding frame. This frame-wall interaction redistributes forces throughout the structure and delays hinge formation in the frame members.

The limited hinge development observed in this model confirms that the shear wall system remains the dominant lateral-force-resisting mechanism throughout most of the analysis.

Case	Peak Base Shear (kN)	Max Roof Disp. (m)	Performance Point Disp.	Performance Point Base Shear	First Hinge Step	First Hinge Location	First Hinge Member
X-Tri	884244	0.166	0.008	48376	2nd	various	beams & columns
X-Uni	1321543	0.127	4.50E-03	60500	1st	19th storey	beams
X-Modal	1037942	0.107	0.00538	59872	1st	10th storey	beams
Y-Tri	684244	0.128	0.0081	48284	1st	10th storey	beams
Y-Uni	904180	0.0786	4.56E-03	60552	1st	10th & 19th	beams
Y-Modal	750000`	0.0761	5.46E-03	59741	1st	10th storey	beams

Fig. 44: Load Pattern Results for G+20 Shear Wall Core Building

5.2.5 G+20 Perimeter Shear Wall Building

1. Uniform loading pattern calculations:
   Uniform load (Q_i) = base shear/number of storeys
   Q_i = 499.1/21
   Therefore, Q_i = 23.76 kN for each storey.

2. parabolic loading pattern calculations:
   parabolic load
   $$Q_i = V_B\left[\frac{W_i h_i^2}{\sum_{j=1}^{n} W_j h_j^2}\right]$$
   Q_{21} = 499.1*(2E+06/3E+07)
   Q_{21} = 35.06 kN for the roof joint.

3. Modal loading pattern calculation:
   $Q_{21} = V_B * [(W_{21}*\phi_{21})/\sum W_{21}*\phi_{21})$
   = 499.1*[(14.87/307.19)]
   = 24.16 kN for the roof joint.

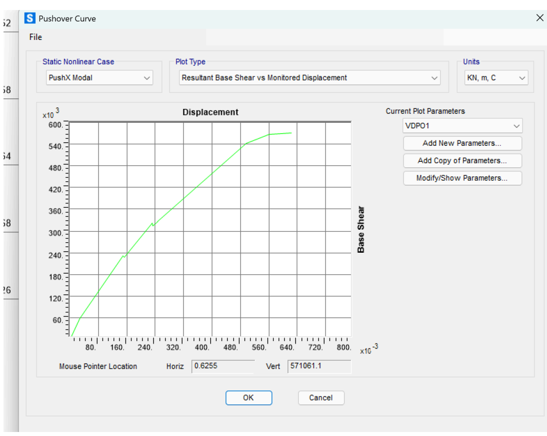

Fig. 45: PushX Modal

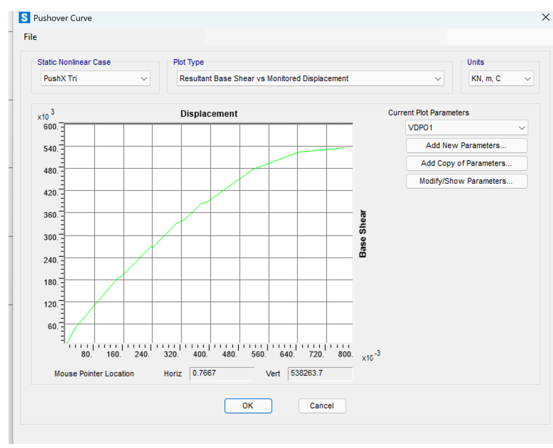

Fig. 46: PushX Parabolic

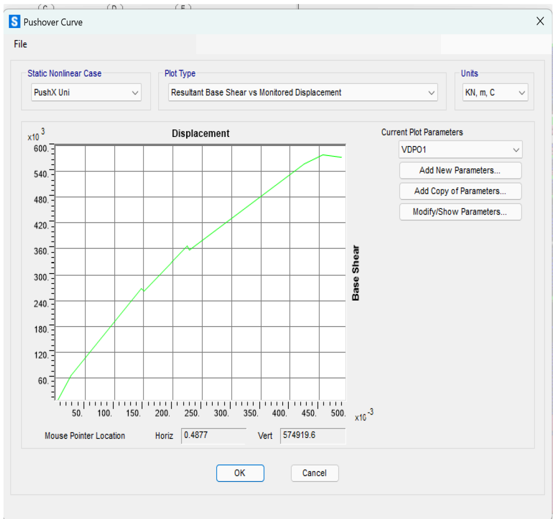

Fig. 47: PushX Uniform

Discussion

The perimeter shear wall system exhibits behavior intermediate between the regular frame and the core wall configuration. The perimeter walls provide significant lateral stiffness while simultaneously allowing greater participation of the frame in resisting seismic forces.

Unlike the core wall model, force transfer occurs through a wider structural footprint, resulting in a more distributed lateral load-resisting mechanism. Consequently, hinge formation is less concentrated, and damage is distributed more uniformly throughout the structure.

An important observation is the development of hinges in the upper storeys above the wall termination region. Since the perimeter walls do not extend into the upper setback portion of the building, the frame becomes the primary lateral-force-resisting system above this level. This sudden transition in stiffness causes increased demand on beams and columns located near the wall termination, explaining the appearance of hinges around the thirteenth and fourteenth storeys.

The perimeter wall system, therefore, provides a balance between stiffness and ductility, offering improved drift control while avoiding the highly concentrated force transfer associated with a single central core.

Case	Peak Base Shear (kN)	Max Roof Disp. (m)	Performance Point Disp.	Performance Point Base Shear	First Hinge Step	First Hinge Location	First Hinge Member
X-Tri	538263	0.7667	0.011	19573	2nd	13th & 14th	beams
X-Uni	574919	0.4877	8.70E-03	22356	1st	13th storey	beams
X-Modal	571061	0.6255	0.0097	20753	1st	13th storey	beams
Y-Tri	553697	0.7745	0.011	19573	1st	13th & 14th	beams
Y-Uni	589067	0.5926	0.00873	22322	1st	13th storey	beams
Y-Modal	528617	0.5662	0.00964	20712	1st	13th storey	beams

Fig. 48: Load Pattern Results for G+20 Perimeter Shear Wall Model

5.3 Performance Point Results

Case	Performance Point Disp.	Performance Point Base Shear
X-Tri	0.027	25767.31
X-Uni	0.017	27120
X-Modal	0.023	26363
Y-Tri	0.027	25767
Y-Uni	0.017	27120
Y-Modal	0.023	26363

Fig. 49: Performance Point (PP) Results for G+15 Model

Case	Performance Point Disp.	Performance Point Base Shear
X-Tri	0.049	42858.704
X-Uni	0.034	45826.826
X-Modal	0.041	44261.686
Y-Tri	0.049	42858.704
Y-Uni	0.034	45826.826
Y-Modal	0.041	44173.47

Fig. 50: PP Results for G+20 Model

Case	Performance Point Disp.	Performance Point Base Shear
X-Tri	0.029	32912
X-Uni	0.022	36289
X-Modal	0.025	34219
Y-Tri	0.029	32912
Y-Uni	0.022	36281
Y-Modal	0.025	34212

Fig. 51: PP Results for G+20 Irregular Model

Case	Performance Point Disp.	Performance Point Base Shear
X-Tri	0.008	48376
X-Uni	4.50E-03	60500
X-Modal	0.00538	59872
Y-Tri	0.0081	48284
Y-Uni	4.56E-03	60552
Y-Modal	5.46E-03	59741

Fig. 52: PP Results for G+20 Shear Wall Core Model

Case	Performance Point Disp.	Performance Point Base Shear
X-Tri	0.011	19573
X-Uni	8.70E-03	22356
X-Modal	0.0097	20753
Y-Tri	0.011	19573
Y-Uni	0.00873	22322
Y-Modal	0.00964	20712

Fig. 53: PP Results for G+20 Perimeter Shear Wall Model

Discussion

The performance point represents the expected structural response under the design earthquake. Buildings possessing higher lateral stiffness exhibited smaller performance point displacements, whereas flexible structures experienced larger displacement demands. The shear wall models demonstrated significantly reduced performance point displacements due to increased stiffness and enhanced resistance against lateral deformation.

5.4 Hinge Formation and Damage Progression

5.4.1 G+15 Regular Building

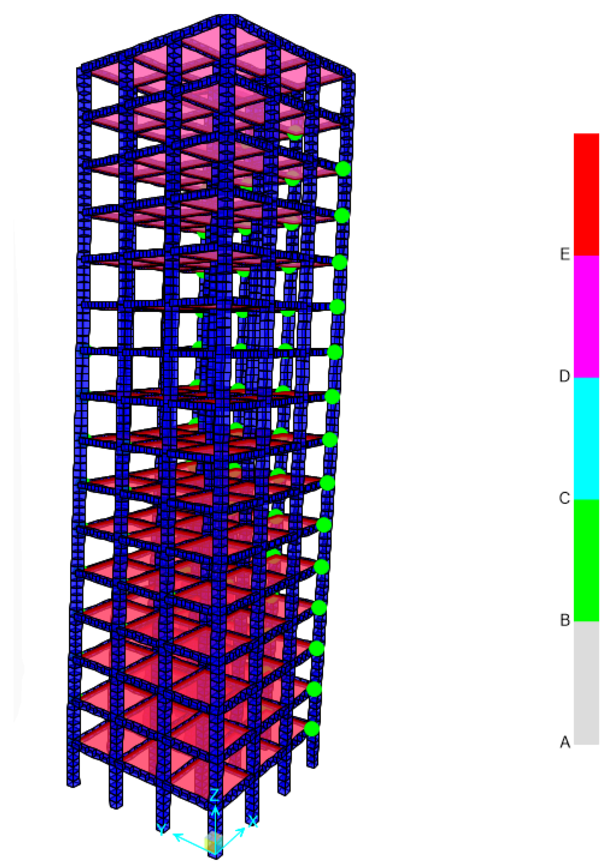

Fig. 54: First Hinge formation under PushX parabolic Loading in Model 1

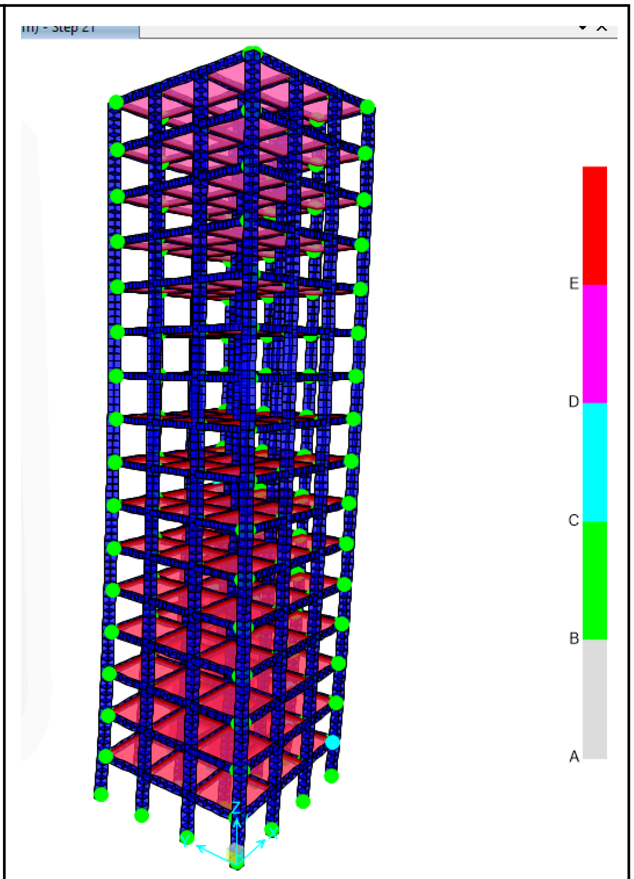

Fig. 55: Last Hinge formation under PushX parabolic Loading in Model 1

Case	First Hinge Step	First Hinge Location	First Hinge Member
X-Tri	4th	various	beam
X-Uni	2nd	various	beams
X-Modal	2nd	various	beams
Y-Tri	1st	5, 6, 7 storey	Beams
Y-Uni	1st	4th storey	beams
Y-Modal	1st	4th 5th storey	beams

Fig. 56: Hinge formation in all load cases for G+15 Regular Building (Model 1)

Discussion

In the G+15 regular frame building, plastic hinge formation for load case X parabolic initiated at the fourth step in the beams at various storeys due to the concentration of bending moments near the beams at each level.

5.4.2 G+20 Regular Building

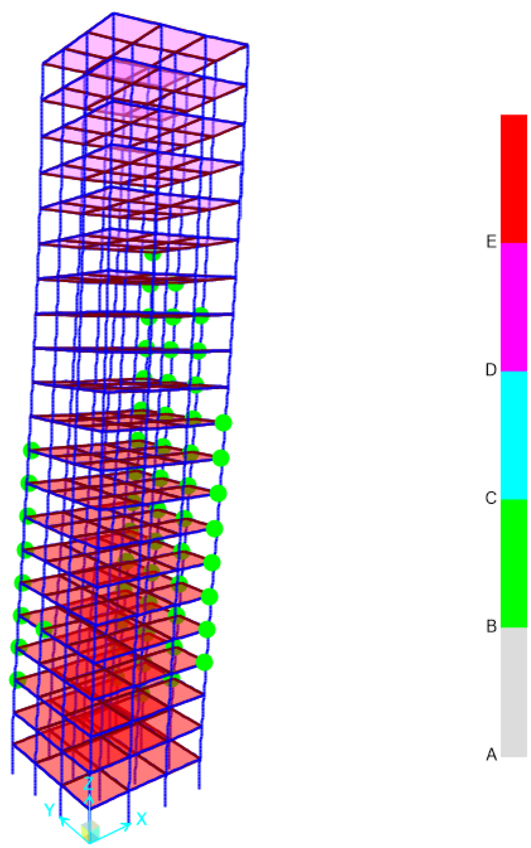

Fig. 57: First Hinge formation under PushX parabolic Loading in Model 2

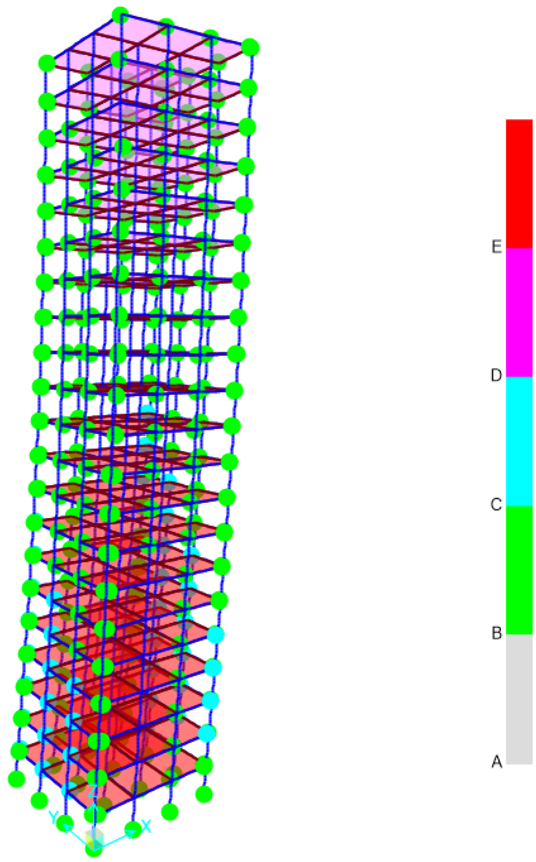

Fig. 58: Last Hinge formation under PushX parabolic Loading in Model 2

Case	First Hinge Step	First Hinge Location	First Hinge Member
X-Tri	2nd	various	beams
X-Uni	1st step	5th & 6th	beams
X-Modal	1st step	6th & 7th	beams
Y-Tri	2nd	various	beams
Y-Uni	1st step	5th & 6th	beams
Y-Modal	1st step	5th & 6th	beams

Fig. 59: Hinge formation in all load cases for G+20 Regular Building (Model 2)

Discussion

In the G+20 regular frame building, plastic hinge formation for load case X parabolic initiated at the second step in the beams at various storeys due to the concentration of bending moments near the beams at each level.

5.4.3 G+20 Setback Building

Case	First Hinge Step	First Hinge Location	First Hinge Member
X-Tri	2nd	various	beams
X-Uni	2nd	various	beams
X-Modal	1st	10th storey	beams
Y-Tri	1st	10th storey	beams
Y-Uni	1st	10th storey	beams
Y-Modal	1st	10th storey	beams

Fig. 60: Hinge formation in all load cases for G+20 irregular Building (Model 3)

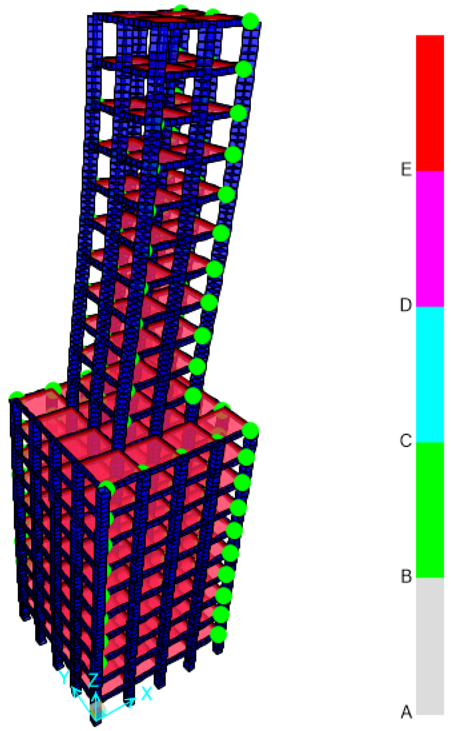

Fig. 61: First Hinge formation under PushX parabolic Loading in Model 3

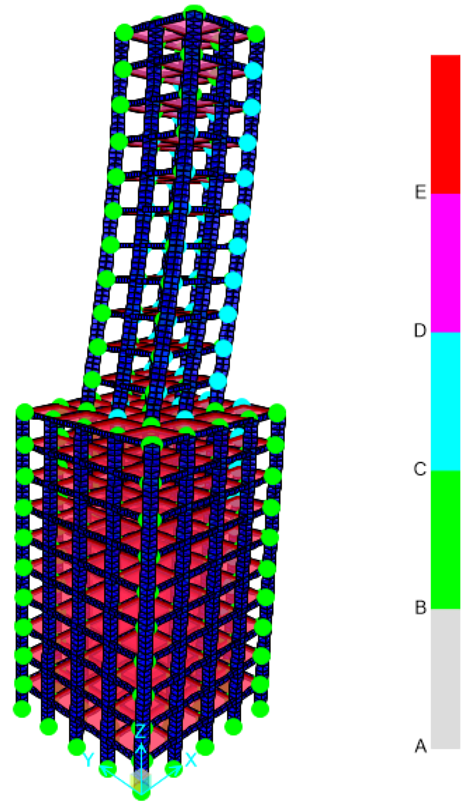

Fig. 62: Last Hinge formation under PushX parabolic Loading in Model 3

Discussion

In the G+20 irregular frame building, plastic hinge formation for load case X parabolic initiated at the second step in the beams at various storeys due to the concentration of bending moments near the beams at each level.

Most of the hinges in all load cases remained in the Immediate Occupancy performance level, while some moved into the Life Safety and even Collapse Prevention levels.

The setback building exhibited a concentration of plastic hinges near the setback transition region. Initial hinge formation for all other load cases occurred at the 10th storey (the setback level), indicating stiffness discontinuity and stress concentration in the vicinity of geometric irregularity. The behaviour confirms the adverse influence of vertical irregularity on seismic performance.

5.4.4 Core Shear Wall Building

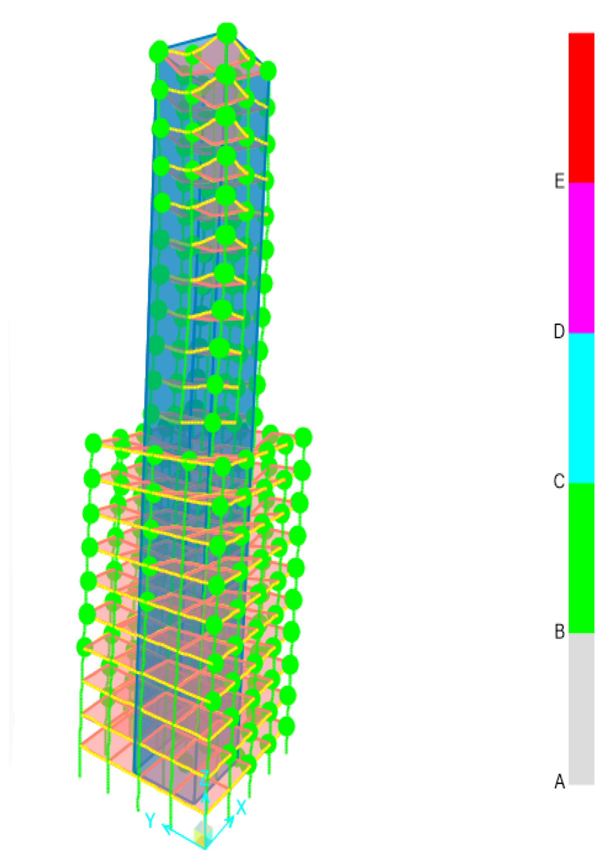

Fig. 63: First Hinge formation under PushX parabolic Loading in Model 4

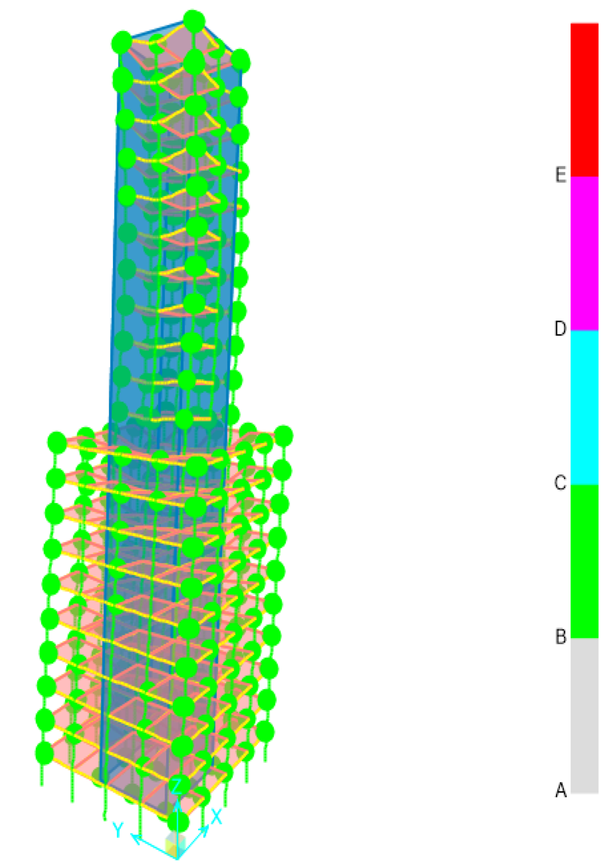

Fig. 64: Last Hinge formation under PushX parabolic Loading in Model 4

Discussion

In the G+20 shear wall core building, plastic hinge formation for load case X parabolic initiated at the second step in the beams at various storeys due to the concentration of bending moments near the beams at each level.

Most of the hinges in all load cases remained in the Immediate Occupancy performance level, while none moved into the Life Safety and Collapse Prevention levels. Because the shear wall carried most of the lateral force, preventing the displacement in the setback stories, which prevented critical hinge formation.

In this model, very few hinge steps were observed as compared to other models. And as results show, this model has a large capacity for bearing the lateral earthquake forces because of the central shear wall.

Case	First Hinge Step	First Hinge Location	First Hinge Member
X-Tri	2nd	various	beams & columns
X-Uni	1st	19th storey	beams
X-Modal	1st	10th storey	beams
Y-Tri	1st	10th storey	beams
Y-Uni	1st	10th & 19th	beams
Y-Modal	1st	10th storey	beams

Fig. 65: Hinge formation in all load cases for G+20 Shear Wall Core Building (Model 4)

5.4.5 Perimeter Shear Wall Building

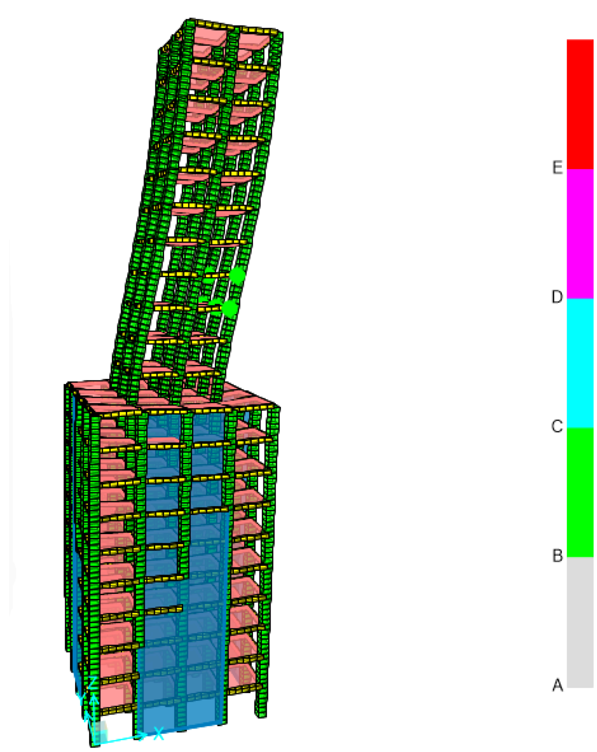

Fig. 66: First Hinge formation under PushX parabolic Loading in Model 5

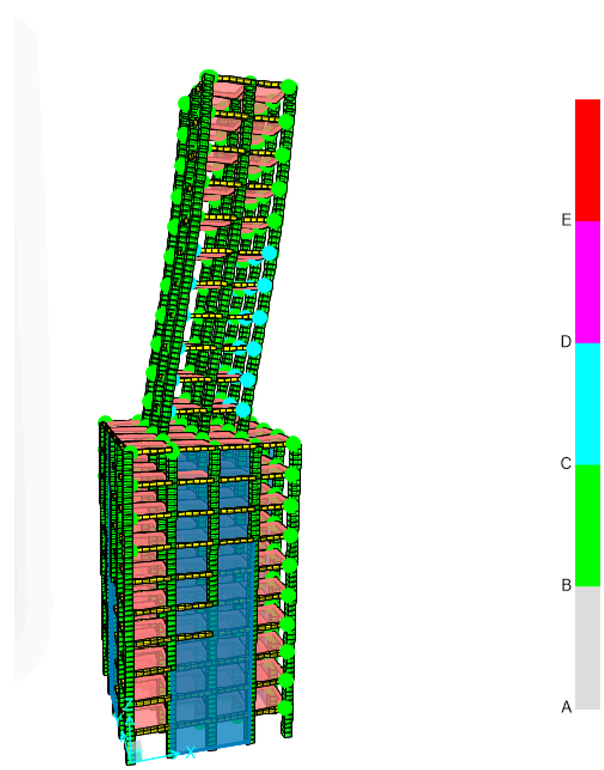

Fig. 67: Last Hinge formation under PushX parabolic Loading in Model 5

Case	First Hinge Step	First Hinge Location	First Hinge Member
X-Tri	2nd	13th & 14th	beams
X-Uni	1st	13th storey	beams
X-Modal	1st	13th storey	beams
Y-Tri	1st	13th & 14th	beams
Y-Uni	1st	13th storey	beams
Y-Modal	1st	13th storey	beams

Fig. 68: Hinge formation in all load cases for G+20 Perimeter Shear Wall Building (Model 5)

Discussion

In the G+20 perimeter shear wall building, plastic hinge formation for load case X parabolic initiated at the second step in the beams at 13th and 14th storeys due to the concentration of bending moments near the beams at each level.

Most of the hinges in all load cases remained in the Immediate Occupancy performance level below the setback where there was a perimeter shear wall, while some moved into the Life Safety level. Because the shear wall carried most of the lateral force at the floors below the setback, preventing the displacement in the lower stories, which prevented critical hinge formation.

In this model, very few hinge steps were observed as compared to other models. And as results show, this model has a large capacity for bearing the lateral earthquake forces at the lower stories because of the perimeter shear wall.

5.5 Hinge Distribution Comparison

Table 5.1 Comparison of Critical Hinge Regions

Model	First Hinge Location	Dominant Damage Region
G+15 Regular	Beams	Lower Storeys
G+20 Regular	Beams	Lower Storeys
G+20 Setback	Beams in setback	Setback Zone
Core Wall	Limited Hinges	Localized Regions
Perimeter Wall	Distributed	Setback Region

Discussion

Comparison of hinge distribution reveals significant variation in damage concentration among structural configurations. The regular buildings primarily developed hinges at the lower storeys, while the setback building exhibited damage concentration near the geometric discontinuity. Shear wall systems substantially reduced hinge formation by resisting a major portion of the lateral load, thereby improving overall seismic performance.

The pushover analysis showed that hinge formation initiated predominantly between the 11th and 15th storeys, corresponding closely to the setback region identified as vertically irregular according to IS 1893:2016. This confirms that the geometric discontinuity significantly influenced the nonlinear response of the structure.

Table 5.2: Master Comparison Table

Model	Max RS Base Shear (kN)	Overstrength (Ω)	PP Disp. (m)	PP Base Shear (kN)	Response Reduction R_μ	Ductility (μ)
G+15	326.292	1.370	0.027	25707.31	4.71	4.71
G+20	346.44	1.306	0.049	42858.7	5.71	5.71
G+20 Irregular	363.55	1.479	0.029	32912	2.75	2.75
G+20 CSW	1035.83	1.960	0.008	48376	2.15	2.15
G+20 PSW	1501.6	3.402	0.011	19573	4.84	4.84

CHAPTER 6
SEISMIC PERFORMANCE EVALUATION

6.1 Introduction

The nonlinear pushover analysis presented in Chapter 5 provides information regarding the strength and deformation characteristics of the investigated building models. However, a more comprehensive evaluation of seismic performance requires assessment of ductility, overstrength, section behaviour, and expected performance levels under different earthquake intensities.

This chapter evaluates the seismic performance of all building models through ductility analysis, overstrength assessment, moment-curvature behaviour of representative structural members, and performance-based classification using a performance matrix. The results provide a deeper understanding of the ability of each structural system to resist earthquake loading beyond the elastic range.

6.2 Ductility Evaluation

Ductility is one of the most important parameters governing the seismic performance of structures. It represents the ability of a structure to undergo significant inelastic deformation without experiencing sudden failure. Structures possessing higher ductility can dissipate greater amounts of earthquake energy and are therefore considered more resilient during strong ground motion.

The displacement ductility ratio was calculated using the ratio of ultimate displacement to yield displacement obtained from the pushover capacity curves.

Ductility (μ) = ultimate displacement/yield displacement

$$\mu = \Delta u/\Delta y$$

The calculated ductility ratios for all building models are presented in Table 6.1.

Yield displacement was approximated from the onset of significant stiffness degradation observed in the pushover curve. Due to the absence of a distinct yield plateau in several models, an exact equal-energy bilinearization was not performed.

Table 6.1: Ductility Table

Model	Δy (m)	Δu (m)	μ
G+15 Regular	0.15	0.7078	4.718
G+20 Regular	0.1765	1.008	5.711
G+20 Setback	0.7	1.926	2.75
G+20 Core Wall	0.077	0.166	2.155
G+20 Perimeter Wall	0.16	0.7745	4.84

Discussion

The G+20 regular building model had the highest ductility, mostly because tall buildings naturally exhibit higher global ductility—the ability to bend and sway without collapsing—because their significant height-to-width ratio increases their fundamental vibration period. This flexibility helps them act as shock absorbers, safely dissipating the immense kinetic energy caused by earthquakes.
Since taller structures are more flexible, they have a larger fundamental time period when seismic waves hit, a longer period shifts the building away from the most destructive, high-frequency earthquake vibrations, reducing the sudden forces it has to absorb.

Similarly, the G+20 Core shear wall model displayed the lowest ductility because of the shear wall core, which made the building more rigid despite its height. Hence, it reduced the flexibility of the building, resulting in a lower fundamental time period.

In the next model, where the shear walls for the upper floors in the setback building were removed, it showed an increase of almost 100% in the ductility, displaying that the shear wall did play a significant role in the structure's overall stability and flexibility.

The regular frame buildings exhibited higher displacement ductility due to greater flexibility and larger inelastic deformation capacity. The shear wall models showed lower displacement ductility but significantly higher stiffness and strength. The setback building demonstrated reduced ductility because of stress concentration near the geometric discontinuity.

Applicability of the Equal Displacement Rule

The ductility reduction factor (R_μ) was evaluated using the Equal Displacement Rule, according to which the ductility-related component of the response reduction factor may be approximated as:

$R_\mu = \mu$

This assumption is generally applicable to structures whose fundamental period exceeds the corner period of the design response spectrum. For medium soil conditions specified in IS 1893 (Part 1): 2016, the corner period is approximately 0.55 seconds.

The fundamental periods obtained from modal analysis for all investigated building models ranged from approximately 1.32 seconds to 2.83 seconds, which are significantly greater than the corner period of the design spectrum. Therefore, the Equal Displacement Rule is considered applicable, and the approximation ($R_\mu = \mu$) has been adopted in the present study.

Consequently, the overall response reduction factor was evaluated using the relationship:
$R = R_S * R_\mu$

where (R_S) represents the overstrength component and (R_μ) represents the ductility component.

Table for Verification of Equal Displacement Rule

Model	Time Period (s)	Corner Time (s)	T > Tc?	ED Rule Apply?
G+15	2.031	0.55	Yes	Yes
G+20	2.837	0.55	Yes	Yes
G+20 Irregular	2.071	0.55	Yes	Yes
G+20 CSW	1.320	0.55	Yes	Yes
G+20 PSW	1.602	0.55	Yes	Yes

6.3 Overstrength Evaluation

Overstrength represents the reserve strength available in a structure beyond the design strength considered during seismic design. It accounts for factors such as material overcapacity, redundancy, strain hardening, and conservatism in design assumptions.

The overstrength factor was evaluated using the ratio of the maximum base shear obtained from response spectrum analysis to the design base shear obtained from seismic design calculations.

Overstrength (Ω) = Maximum base shear/design base shear

$$\Omega = V_{max}/V_d$$

Higher values of overstrength indicate greater reserve capacity and improved resistance against severe earthquake loading.

Table 6.2: Overstrength Table

Model	Design Base Shear (kN)	Vmax (kN)	Ω
G+15	238.172	326.292	1.369
G+20	346.44	452.75	1.306
G+20 Setback	363.55	538	1.479
G+20 Core Wall	527	1035.83	1.965
G+20 Perimeter Wall	441.38	1501	3.402

G+15 Regular Frame

The G+15 building exhibited an overstrength factor of **1.369**, indicating that the structure could resist approximately **37% more lateral load** than the design demand before reaching its maximum capacity.

The moderate value suggests that the building possesses some inherent redundancy and reserve strength but remains primarily governed by frame action. The absence of shear walls limits the development of substantial additional strength after yielding.

G+20 Regular Frame

The G+20 regular frame produced an overstrength factor of **1.306**, slightly lower than the G+15 model.

This reduction is expected because increasing building height generally increases flexibility and seismic demand while reducing the relative contribution of member overdesign. As plastic hinges develop, the structure experiences only a modest increase in lateral resistance beyond the design base shear.

Although lower than values frequently reported for special moment-resisting frames, the result still indicates the presence of reserve strength and is consistent with a code-designed frame lacking supplemental lateral-force-resisting systems.

G+20 Setback Building

The setback structure achieved an overstrength factor of **1.479**, which is higher than both regular frame models.

This may initially appear counterintuitive because setback irregularities generally reduce seismic performance. However, overstrength reflects strength reserve rather than deformation performance. The concentration of stiffness and strength near the setback region can increase the peak lateral resistance, resulting in a larger Vmax.

Despite the higher overstrength, the setback model exhibited localized hinge concentration and increased displacement demand, indicating that greater strength does not necessarily translate to better seismic behaviour.

G+20 Core Shear Wall Building

The core wall model developed an overstrength factor of **1.965**, nearly twice the design base shear.

The reinforced concrete core significantly increased structural stiffness and contributed substantial lateral resistance. As seismic loading increased, both the frame and the wall participated in resisting the applied forces, enabling the structure to sustain considerably larger base shear levels before significant degradation occurred.

This demonstrates the effectiveness of central shear walls in enhancing seismic reserve capacity and controlling damage.

G+20 Perimeter Shear Wall Building

The perimeter wall system achieved the highest overstrength factor of **3.402**.

This means the structure was capable of resisting more than three times the design base shear before reaching its maximum capacity. Such behaviour is characteristic of highly redundant wall-frame systems in which perimeter walls provide substantial resistance against overturning and lateral deformation.

The distributed wall arrangement mobilizes a larger portion of the building footprint, improving force transfer and reducing stress concentration. Consequently, the perimeter wall model demonstrated the greatest reserve strength among all investigated structures.

Comparative Interpretation

The results indicate that:

1. Regular frame buildings possess the lowest reserve strength, with overstrength factors ranging between 1.3 and 1.4.
2. The setback configuration slightly increases peak strength, but this advantage is offset by poorer deformation characteristics and hinge concentration near the irregularity.
3. Core shear walls nearly double the available reserve strength, significantly improving seismic resistance.
4. Perimeter shear walls provide the highest overstrength, demonstrating the most effective lateral load-resisting mechanism among the investigated systems.

Therefore, from an overstrength perspective:

Perimeter Wall > Core Wall > Setback > G+15 > G+20

The results confirm that the incorporation of shear walls substantially enhances the seismic reserve capacity of reinforced concrete buildings and reduces reliance on frame action alone during strong earthquake excitation.

6.4 Moment-Curvature Study

A Moment-Curvature Study analyzes the relationship between an applied bending moment (M) and the resulting curvature (κ) of a structural member. It is an essential, highly localized assessment tool in structural engineering that models inelastic behavior, ductility, energy dissipation, and stiffness degradation.

Key Phases of the Moment-Curvature Curve

Under increasing load, a reinforced concrete (RC) cross-section transitions through distinct stages:

1. **Uncracked / Elastic Phase:** The behavior is linear. The slope represents the gross flexural rigidity EI_{gross}, extending up until the cracking moment $M_{cr,}$ where tensile stress exceeds the modulus of rupture.
   Here, $M < M_{Cr}$
2. **Cracked / Linear Elastic Phase:** After cracking, the concrete in tension is ignored. The curve continues linearly—but with reduced stiffness—until the reinforcing steel yields.
   Here, $M_{Cr} < M < M_y$
3. **Yield Phase:** The steel yields, causing the curvature to increase significantly while the bending moment increases only slightly or not at all.
   Here, $M = M_y$ and $\phi = \phi_y$
4. **Ultimate Phase:** The concrete reaches its maximum usable compressive strain (e.g., ≈ 0.003 for unconfined concrete). The curve drops or levels off, indicating crushing or failure.
   Here, $M = M_U$ and $\phi = \phi_U$

The study of the Moment-Curvature Curve was performed for only one representative column and one representative beam used in the structural modelling in this project.

6.4.1 Column Section

The column section was designed for the P-M2-M3 design using Fe415 as the rebar material and M35 as the concrete material. The dimensions of the columns were 800x800 mm.
The type of confinement used was ties.

Clear Cover for Confinement Bars: 40 mm.
Number of Longitudinal Bars: 5 in each direction.
Size of Longitudinal bar: #11 or 35.81 mm

Confinement Bar Size: #4
Longitudinal spacing of confinement bars: 0.15
Number of confinement bars: 4 in each direction.

The reinforcement is to be checked.

Parameter	Value
Width	800 mm
Depth	800 mm
Cover	40 mm
Concrete Grade	M35
Steel Grade	Fe415
Maximum Axial Load	-1833 kN

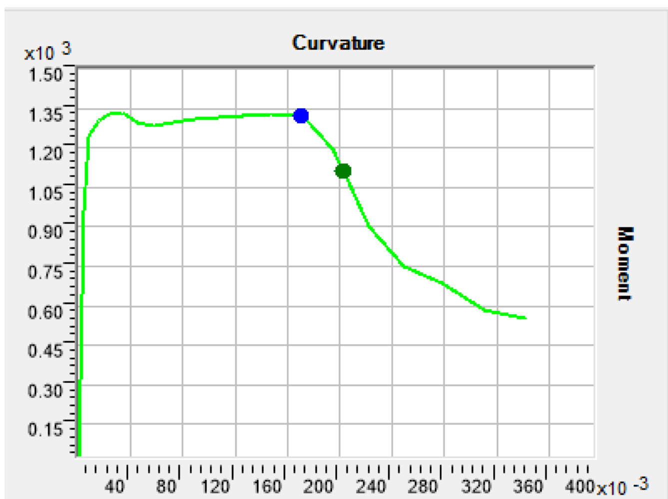

Fig. 69: Moment-Curvature Curve for Column with axial load (P) = -1833 kN

Table for Moment-Curvature Parameters for Column:

Parameter	Value
Yield Moment (My)	1011.1928
Ultimate Moment (Mu)	551.063
Yield Curvature (φy)	4.068E-03
Ultimate Curvature (φu)	0.3425
Curvature Ductility (μφ)	41.9

Discussion

Notice that the yield moment (M_y) is greater than the ultimate moment (M_u). This indicates that the column has undergone heavy strain softening (the loss of strength) due to concrete crushing at this ultimate stage.

Also, the curvature ductility value μ_φ was obtained to be 41.9. A ductility value this high indicates that the Mander-confined column model is working exceptionally well, which is exactly what we need to safely handle seismic drift and torsion in an irregular high-rise building.

6.4.2 Beam Section

The beam section was designed for the M3 design only, using Fe415 as the rebar material and M30 as the concrete material. The dimensions of the beams were 300x400 mm.
The type of confinement used was ties.

Parameter	Value
Width	300 mm
Depth	400 mm
Cover on top & bottom	60 mm & 50 mm
Concrete Grade	M30
Steel Grade	Fe415

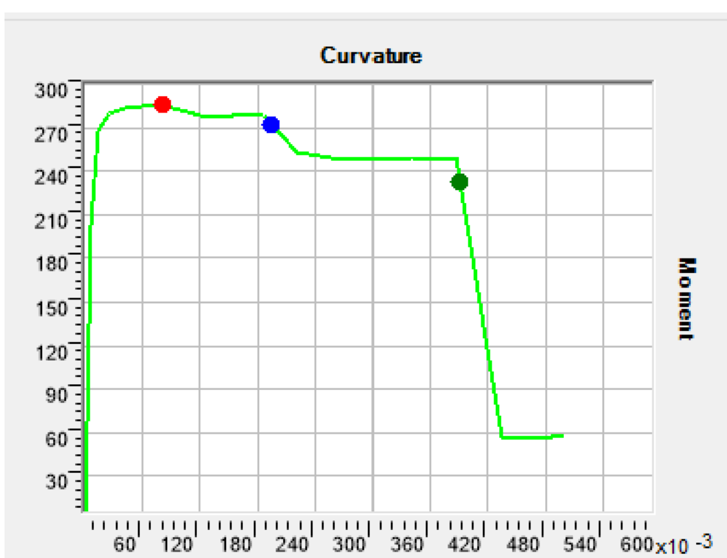

Fig. 70: Moment-Curvature Curve for Beam

Table for Moment-Curvature Parameters for Beam:

Parameter	Value
Yield Moment (My)	207
Ultimate Moment (Mu)	57.1345
Yield Curvature (φy)	6.182E-03
Ultimate Curvature (φu)	0.5007
Curvature Ductility (μφ)	81

Discussion

Notice that the yield moment (M_y) is greater than the ultimate moment (M_u) here too. This indicates that the concrete in the beam has undergone heavy strain softening (the loss of strength) due to beam crushing at this ultimate stage.

Also, the curvature ductility value μ_φ was obtained to be 81. A ductility value this high indicates that the Mander-confined beam model is working exceptionally well, which is exactly what we need to safely handle seismic drift and torsion in an irregular high-rise building.

Table for Validation of SAP2000 Hinge Properties

Beam Section

Parameter	Moment-Curvature	SAP Hinge
Yield Moment (kN-m)	207	128.6

Difference: [(SAP Hinge yield moment - moment-curvature yield moment)/SAP hinge yield moment]*100

= [(207-128.6)/207]*100

= 37.87%

Column Section

Parameter	Moment-Curvature	SAP Hinge
Yield Moment (kN-m)	1011.192	1820.466

Difference: [(SAP Hinge yield moment - moment-curvature yield moment)/SAP hinge yield moment]*100

= [(1820.466-1011.192)/1820.466]*100

= 44.41%

The discrepancy in the values of SAP hinge yield moment and the yield moment obtained from the moment-curvature curve arises because SAP2000 auto-hinge properties are generated using generalized ASCE 41-17 parameters, whereas the moment-curvature analysis explicitly considers the reinforcement configuration and material nonlinearities of the selected section. Nevertheless, the values remain within an acceptable range for nonlinear performance assessment.

6.4.3 Four-Phase Moment-Curvature Curve

The figure 71 below shows the four phases in the achieved moment-curvature curve for the column section.

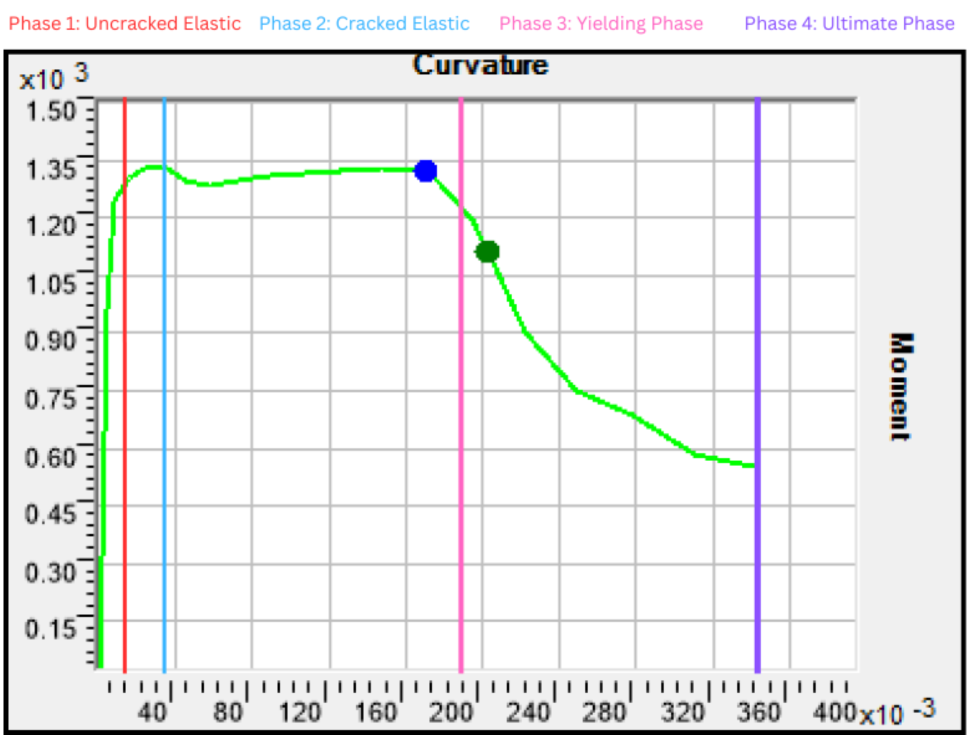

Fig. 71: Four Phases of Moment-Curvature Curve

Where the red line shows Phase 1: Uncracked Elastic Phase. This is the safest elastic phase, where the concrete is uncracked, there is a linear relationship between load and deformation, and this is where the highest stiffness is observed in the structural components.

The blue line shows Phase 2: Cracked Elastic. The behaviour shown in this phase includes cracking in concrete due to tension, a reduced stiffness, and the reinforcement starts carrying tensile load.

The pink line shows Phase 3: Yielding Phase. This phase is generally where the steel starts yielding, and plasticity initiates.

The purple line at the end shows Phase 4: The Ultimate Phase. In this phase, the structural components have reached their maximum capacity, and the concrete is crushed, or the reinforcements have failed.

6.4.4 Plastic Hinge Length

Use Paulay & Priestley:

$$L_p = 0.08L+0.022d_bf_y$$

where:

L = member length (mm)

d_b = longitudinal bar diameter (mm)

f_y = steel yield stress (MPa)

Calculations

For Beam in a regular model:
L = 3200 mm
db = 35.81 mm
f_y = 415 MPa

L_p = (0.08*3200) + (0.022*35.81*415)
Therefore, $L_p = 582.94$ *mm*

6.4.5 Curvature Ductility

Using:

$\mu_\phi = \phi_u / \phi_y$ = 190/40
Therefore, μ_ϕ = 4.75

Where, ϕ_u = ultimate curvature
Φ_y = yield curvature

6.5 Performance Matrix

Performance Levels

Level	Meaning
IO	Immediate Occupancy
LS	Life Safety
CP	Collapse Prevention

Earthquake Levels

Hazard Level	Description
Frequent EQ	Service Earthquake
Design EQ	DBE
Rare EQ	MCE

- A frequent earthquake was assumed as 50% DBE demand.
- Design earthquake corresponds to ATC-40 performance point.
- Rare earthquake assumed as approximately 150–200% DBE demand based on hinge progression beyond the performance point.

Table 6.3: Performance Matrix

Model	Frequent EQ	Design EQ	Rare EQ
G+15 Regular	IO	IO	IO-LS
G+20 Regular	IO	IO	IO-LS
Setback	IO	IO	LS-CP
Core Wall	IO	IO	IO-LS
Perimeter Wall	IO	IO	LS-CP

Table 6.3 presents the performance matrix developed from the ATC-40 performance point results and observed hinge progression during pushover analysis. All building models remained

within the Immediate Occupancy performance level at the design earthquake demand, indicating adequate seismic resistance under code-specified loading conditions.

However, differences emerged when the structures were subjected to increasing displacement demands. The setback building exhibited Collapse Prevention behaviour due to the concentration of plastic hinges near the setback region, whereas the regular and shear wall structures maintained Life Safety performance.

The results demonstrate that geometric irregularity adversely affects seismic performance, while the inclusion of shear walls improves structural stability and damage control.

6.6 Derived Response Reduction Factor

The response reduction factor represents a structure's ability to dissipate seismic energy through a combination of ductility and reserve strength. In the present study, the response reduction factor was estimated using:

$R = R_\mu \times \Omega$

where R_μ represents the ductility-based reduction factor, and Ω represents the overstrength factor.

The derived values were compared with the response reduction factor of R = 5 specified by IS 1893 for Special Moment Resisting Frames (SMRF).

Table for Derived Response Reduction Factor (R)

Model	R_μ	Overstrength (Ω)	Derived R
G+15	4.71	1.369	6.448
G+20	5.71	1.306	7.457
G+20 Irregular	2.75	1.479	4.067
G+20 CSW	2.15	1.965	4.224
G+20 PSW	4.84	3.402	16.465

The **G+15 regular frame** produced a derived response reduction factor of **6.448**, which exceeds the value of **R = 5** prescribed by IS 1893 for Special Moment Resisting Frames (SMRF). This indicates that the structure possesses adequate ductility and reserve strength to dissipate seismic energy beyond the level assumed by the code.

The **G+20 regular frame** exhibited the highest response reduction factor among the frame-dominated systems, with a value of **7.457**. The increase is primarily due to the high ductility developed during the nonlinear response. Despite having relatively modest overstrength, the structure compensated through significant deformation capacity, resulting in a derived R value substantially greater than the code assumption.

The **G+20 irregular (setback) building** achieved a derived response reduction factor of only **4.067**, which is below the code value of 5. The reduction is attributed to stiffness discontinuity and deformation concentration at the setback level. Although the structure retained moderate overstrength, the irregularity significantly reduced its ability to dissipate seismic energy through distributed plastic deformation. This finding suggests that the actual seismic performance of setback buildings may be overestimated when they are assigned the same response reduction factor as regular structures.

The **G+20 Core Shear Wall (CSW)** model produced a derived response reduction factor of **4.224**, which is also lower than the code value. However, unlike the setback structure, this reduction is not caused by poor seismic behavior. The core wall system exhibits very high stiffness and strength, resulting in smaller nonlinear deformations and reduced ductility demand. Consequently, the ductility component of R decreases even though the structure remains highly resistant to lateral loads. The lower R therefore reflects a stiffness-controlled response rather than inadequate seismic performance.

The **G+20 Perimeter Shear Wall (PSW)** model exhibited an exceptionally high derived response reduction factor of **16.465**, far exceeding all other models. This result is primarily driven by the combination of high ductility and extremely large overstrength. The distributed wall arrangement allows efficient lateral load transfer throughout the structural perimeter while simultaneously maintaining significant deformation capacity. The resulting response demonstrates the strong synergistic interaction between the moment-resisting frame and the perimeter wall system.

The exceptionally high response reduction factor obtained for the perimeter shear wall model indicates the combined influence of significant overstrength and ductility.
However, the value should be interpreted with caution. In the present study, the shear walls were modeled as elastic shell elements without explicit nonlinear wall hinge definitions. Consequently, cracking, yielding, stiffness degradation, and crushing within the wall system were not directly represented. The absence of nonlinear wall behavior may lead to an overestimation of both reserve strength and deformation capacity, thereby inflating the derived response reduction factor.

Therefore, while the perimeter shear wall system clearly demonstrates superior seismic performance relative to the frame-only configurations, the calculated value of R = 16.47 should be regarded as an upper-bound estimate rather than an exact representation of the actual response reduction capability of the structural system.

Interpretation of Results

The results reveal that different structural systems achieve seismic resistance through different mechanisms:

- Regular frames rely primarily on ductility.
- Core wall systems rely primarily on stiffness and strength.
- Setback structures suffer a reduction in effective energy dissipation due to geometric irregularity.
- Perimeter wall systems benefit from both high overstrength and substantial ductility.

Accordingly, the derived response reduction factors can be ranked as:

PSW > G+20 > G+15 > CSW > Irregular

6.7 Higher-Mode Effects and Applicability of Pushover Analysis

The nonlinear static pushover procedure assumes that the structural response is predominantly governed by the fundamental vibration mode. This assumption is generally reasonable for low- and medium-rise regular structures; however, its accuracy decreases for taller buildings where higher vibration modes contribute significantly to the seismic response.

The investigated G+20 structures possess heights of approximately 63 m and fundamental periods ranging from approximately 1.3 s to 2.8 s. For buildings of this height, higher-mode effects may influence storey shears, inter-storey drifts, and the distribution of plastic hinges along the height. FEMA 440 recognizes that conventional pushover analysis may underestimate seismic demand in taller structures and structures exhibiting significant vertical irregularity.

Among the models considered, the setback building is expected to be most sensitive to higher-mode effects because the abrupt reduction in plan dimensions produces localized stiffness discontinuities and non-uniform deformation patterns. Consequently, the pushover results obtained in the present study should be interpreted as an approximation of structural performance rather than an exact prediction of earthquake response.

Despite these limitations, pushover analysis remains a valuable tool for identifying strength capacity, performance points, hinge formation patterns, and relative differences between structural configurations. The results, therefore, provide meaningful comparative insight into the seismic performance of the investigated buildings, while recognizing that nonlinear time-history analysis would be required for a more rigorous assessment of higher-mode effects.

6.8 Validation and Limitations of the Present Study

The validity of the present investigation is supported by the use of established seismic analysis procedures, including modal analysis, response spectrum analysis, nonlinear static pushover analysis, ATC-40 performance evaluation, and FEMA/ASCE hinge modeling. The observed trends are consistent with established structural behavior, namely increased stiffness due to shear walls, concentration of damage near structural irregularities, and improved lateral resistance in wall-frame systems.

However, several assumptions and limitations should be acknowledged:

1. Fixed-base supports were assumed for all models. Soil-structure interaction effects were not considered and may alter the dynamic characteristics of the buildings.
2. Material nonlinearity was represented using concentrated plastic hinges. Distributed cracking and localized damage mechanisms were not explicitly modeled.
3. Shear walls were modeled using elastic shell elements. Nonlinear wall cracking, crushing, and yielding behavior were therefore not captured directly.
4. The pushover procedure applies monotonically increasing lateral loads and cannot fully reproduce cyclic degradation, stiffness recovery, or load reversals associated with real earthquakes.

CHAPTER 7
CONCLUSIONS AND FUTURE SCOPE

7.1 Conclusions

The present study investigated the nonlinear seismic performance of reinforced concrete buildings with different structural configurations using SAP2000. Five building models consisting of a G+15 regular frame, G+20 regular frame, G+20 setback frame, G+20 core shear wall system, and G+20 perimeter shear wall system were analyzed using modal analysis, response spectrum analysis, and nonlinear static pushover analysis. Based on the results obtained, the following conclusions are drawn:

1. The introduction of vertical irregularity significantly affected seismic performance. The G+20 setback building exhibited concentration of inelastic demand near the setback level, leading to localized hinge formation and reduced global ductility compared with the regular G+20 frame.
2. Shear wall systems substantially improved lateral stiffness and strength. Both the core shear wall and perimeter shear wall configurations developed lower performance point displacements and higher base shear capacities than the conventional moment-resisting frame systems.
3. The core shear wall model exhibited the smallest displacement demand and maintained Immediate Occupancy (IO) performance at the design earthquake performance point, demonstrating excellent stiffness and drift control.
4. The perimeter shear wall model achieved the highest overstrength factor ($\Omega = 3.402$), indicating substantial reserve strength beyond the code design requirements. This model also produced the highest derived response reduction factor among all investigated configurations.
5. Ductility evaluation showed that the regular frame systems possessed greater deformation capacity than the shear wall systems. Although shear walls increased stiffness and strength, their displacement ductility was lower than that of the corresponding moment-resisting frames.
6. Derived response reduction factors obtained from nonlinear analysis showed significant variation among the structural systems. The G+15 and G+20 regular frames produced derived R values greater than the IS 1893 design value of 5.0, indicating adequate reserve capacity. In contrast, the setback building produced a derived R value of approximately 4.07, suggesting that the code assumption of $R = 5$ may overestimate the actual energy dissipation capability of vertically irregular structures.
7. Storey drift results obtained from Project 1 indicated that shear wall systems provided superior drift control compared with frame-only systems. The reduction in lateral displacement demand observed during pushover analysis further confirmed the effectiveness of shear walls in limiting seismic deformations.

8. Hinge formation patterns demonstrated that structural configuration governs damage progression. Regular frames developed distributed plasticity, whereas the setback building exhibited hinge concentration near the irregularity level. Shear wall models showed limited hinge formation due to their increased stiffness and strength.
9. Performance point evaluation using the ATC-40 procedure indicated that all investigated models remained within acceptable performance limits under the considered design earthquake demand. However, significant differences were observed in reserve capacity, deformation demand, and damage distribution among the structural systems.
10. Among the studied configurations, the perimeter shear wall system exhibited the most favorable overall seismic performance due to its combination of high strength, substantial overstrength, acceptable ductility, and efficient force redistribution mechanisms.

7.2 Future Scope

The present study may be extended through the following investigations:

1. Nonlinear time-history analysis using scaled ground motion records compatible with the IS 1893 design spectrum to evaluate the dynamic response of the investigated structures under realistic earthquake excitation.
2. Development of fragility curves using Incremental Dynamic Analysis (IDA) to quantify the probability of exceeding Immediate Occupancy (IO), Life Safety (LS), and Collapse Prevention (CP) performance levels.
3. Investigation of soil-structure interaction effects through flexible foundation modeling and comparison with the fixed-base assumptions adopted in the present study.
4. Inclusion of nonlinear shear wall hinge behavior and distributed plasticity models to obtain a more realistic representation of wall damage progression.

References

[1] A. S. Hari and B. P. Rani, “Seismic Performance of RC Framed Structures with Vertical Single Setback Irregularity,” *International Journal for Research in Applied Science & Engineering Technology (IJRASET)*, vol. 13, no. 11, Nov. 2025.

[2] P. Agrawal and G. Ghosh, “Seismic Performance of Step-back and Set-back Building Resting on Hill-Slope,” *Procedia Structural Integrity*, vol. 70, pp. 113–120, 2025.

[3] M. Aslani and P. Tehrani, “Seismic Response and Collapse Capacity Assessment of Dual RC Buildings with Vertical Irregularities in Shear Walls,” *Scientific Reports*, vol. 15, Article 9966, 2025.

[4] A. Barua, S. Rana, A. H. M. S. Islam, and S. B. Ali, “Seismic Response Assessment of RC Frame-Shear Wall Buildings with Vertical Setback Irregularities,” in *Proceedings of the 8th*

International Conference on Civil Engineering for Sustainable Development (ICCESD 2026), Bangladesh, 2026.

[5] P. K. Das and M. Mallik, "Seismic Response of Setback Building in Hilly Region with Effect of Lift Well," *Materials Research Proceedings*, vol. 48, pp. 225–233, 2025.

[6] S. Lamsal and N. Patel, "Study of Torsional and Stiffness Properties of the RC Buildings with Shear Wall and Steel Bracing with Lateral Loadings," *International Journal for Multidisciplinary Research (IJFMR)*, vol. 5, no. 4, Jul.–Aug. 2023.

[7] Bureau of Indian Standards, *IS 456:2000 – Plain and Reinforced Concrete: Code of Practice*, New Delhi, India: BIS, 2000.

[8] Bureau of Indian Standards, *IS 1893 (Part 1):2016 – Criteria for Earthquake Resistant Design of Structures, Part 1: General Provisions and Buildings*, New Delhi, India: BIS, 2016.

[9] Applied Technology Council, *ATC-40: Seismic Evaluation and Retrofit of Concrete Buildings*, Redwood City, California, USA: Applied Technology Council, 1996.

[10] Federal Emergency Management Agency (FEMA), *FEMA 356: Prestandard and Commentary for the Seismic Rehabilitation of Buildings*, Washington, D.C., USA: FEMA, 2000.

[11] American Society of Civil Engineers, *ASCE/SEI 41-17: Seismic Evaluation and Retrofit of Existing Buildings*, Reston, Virginia, USA: American Society of Civil Engineers, 2017.

[12] Computers and Structures Inc. (CSI), *SAP2000 Integrated Software for Structural Analysis and Design – User Manual*, Berkeley, California, USA: CSI.

[13] Federal Emergency Management Agency (FEMA), *FEMA 440: Improvement of Nonlinear Static Seismic Analysis Procedures*, Washington, D.C., USA: FEMA, 2005.

[14] Federal Emergency Management Agency (FEMA), *FEMA P-58: Seismic Performance Assessment of Buildings*, Washington, D.C., USA: FEMA, 2018.

[15] American Concrete Institute, *ACI 318-19: Building Code Requirements for Structural Concrete*, Farmington Hills, Michigan, USA: ACI, 2019.

Appendices

Appendix A – Building Geometry and Storey Data

Model	Total Height	Total Weight	Building Dimension
G+15 Regular	48 m	14970.047 kN	12x12 m
G+20 Regular	63 m	34007.945 kN	12x12 m
G+20 Irregular	63 m	32470 kN	16x16 m then 8x8m
G+20 CSW	63 m	40617.83 kN	16x16 m then 8x8m
G+20 PSW	63 m	38468.22 kN	16x16 m then 8x8m

Model	Column Size	Beam size	Shear wall size
G+15 Regular	600x600 mm	300x400 mm	none
G+20 Regular	800x800 mm	300x400 mm	none
G+20 Irregular	800x800 mm	300x400 mm	none
G+20 CSW	800x800 mm	300x400 mm	250 mm thick shell
G+20 PSW	800x800 mm	300x400 mm	250 mm thick shell

Appendix B – Capacity Curves and Performance Points

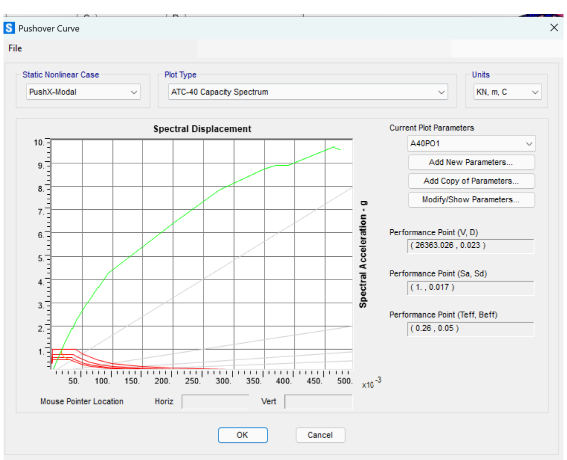

Fig. 72: ATC-40 Curve for PushX Modal G+15 Model

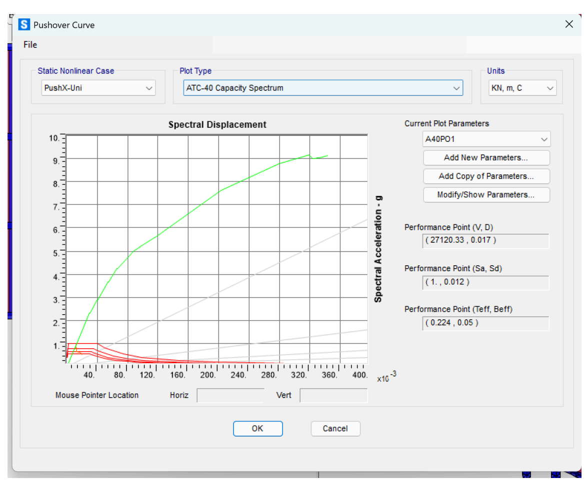

Fig. 73: ATC-40 Curve for PushX Uni G+15 Model

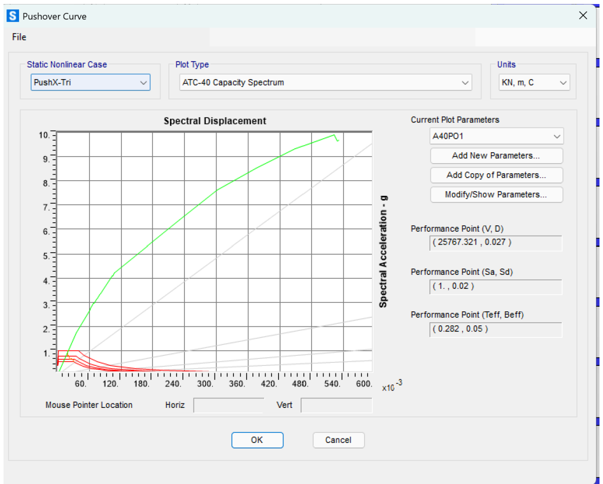

Fig. 74: ATC-40 Curve for PushX Parabolic G+15 Model

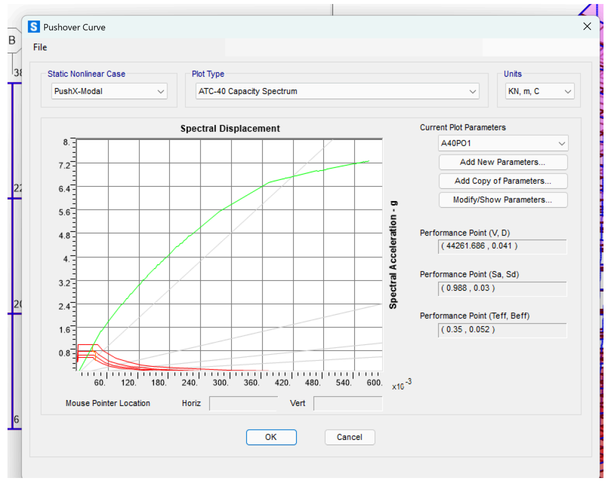

Fig. 75: ATC-40 Curve for PushX Modal G+20 Model

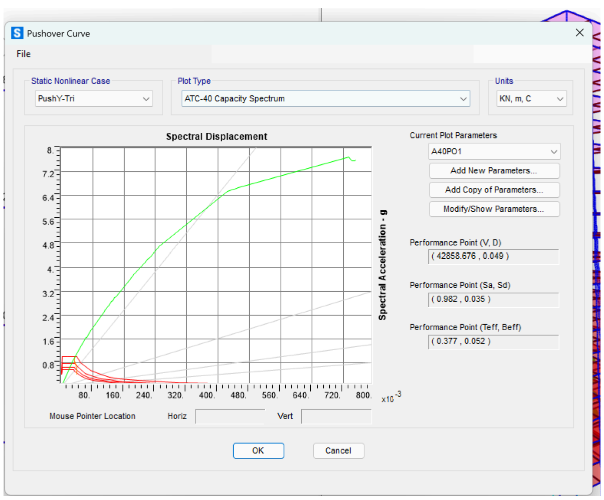

Fig. 76: ATC-40 Curve for PushX Parabolic G+20 Model

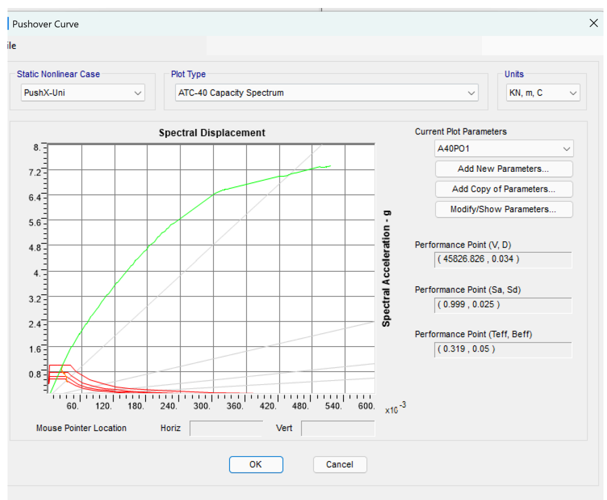

Fig. 77: ATC-40 Curve for PushX Uni G+20 Model

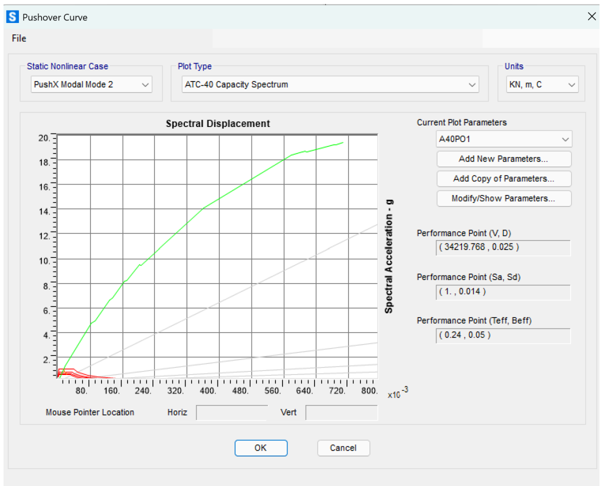

Fig. 78: ATC-40 Curve for PushX Modal G+20 Irregular Model

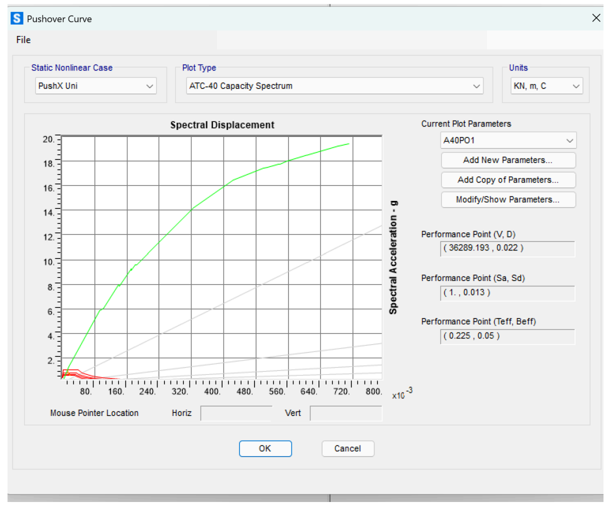

Fig. 79: ATC-40 Curve for PushX Uni G+20 Irregular Model

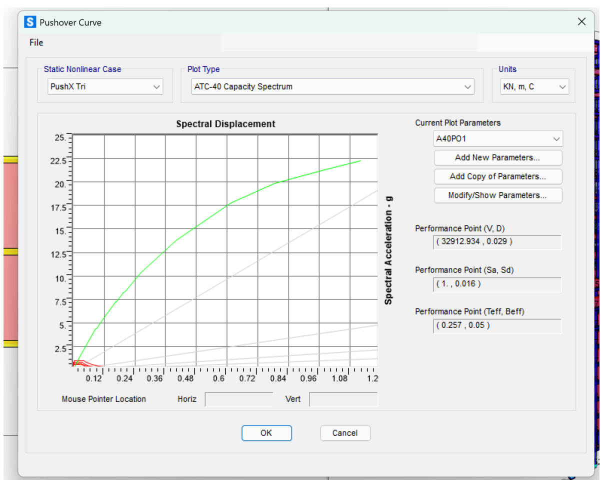

Fig. 80: ATC-40 Curve for PushX Parabolic G+20 Irregular Model

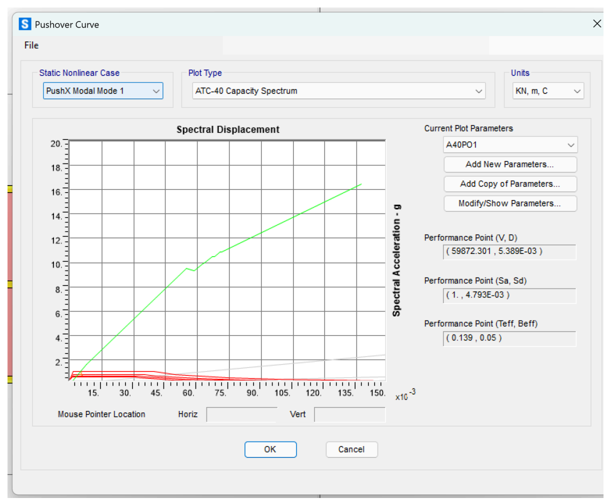

Fig. 81: ATC-40 Curve for PushX Modal G+20 CSW Model

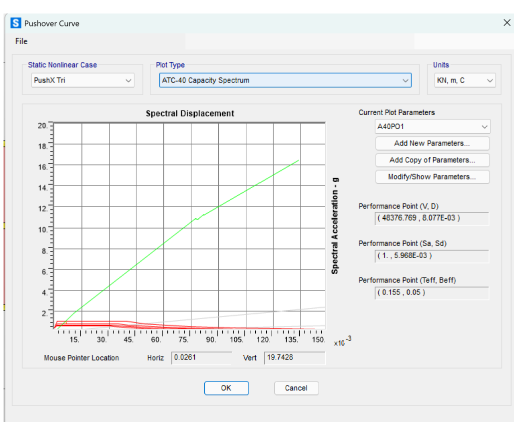

Fig. 82: ATC-40 Curve for PushX Parabolic G+20 CSW Model

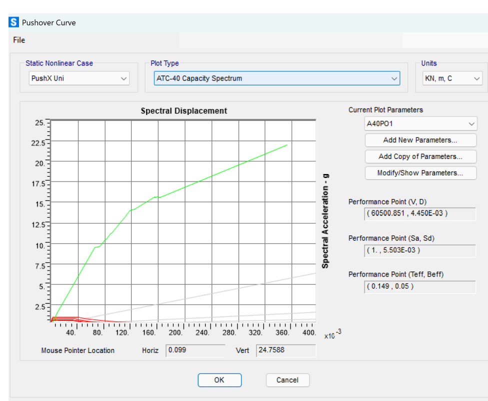

Fig. 83: ATC-40 Curve for PushX Uni G+20 CSW Model

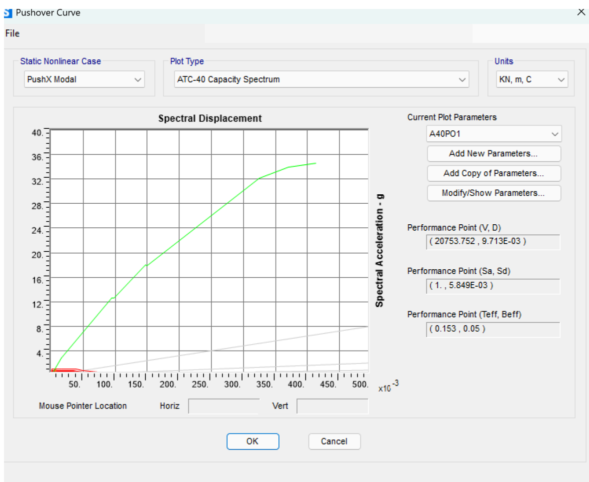

Fig. 84: ATC-40 Curve for PushX Modal G+20 PSW Model

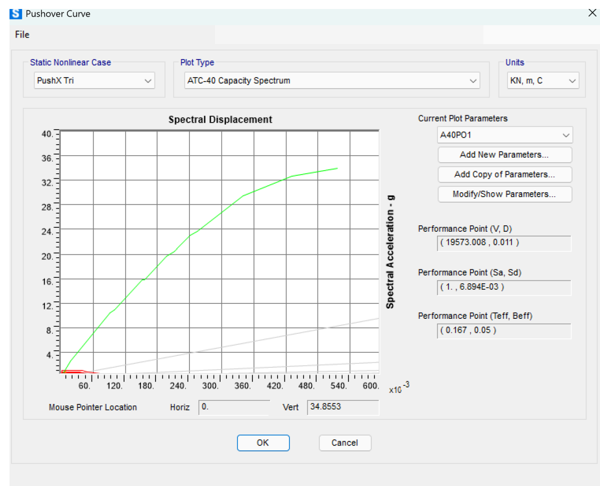

Fig. 85: ATC-40 Curve for PushX Parabolic G+20 PSW Model

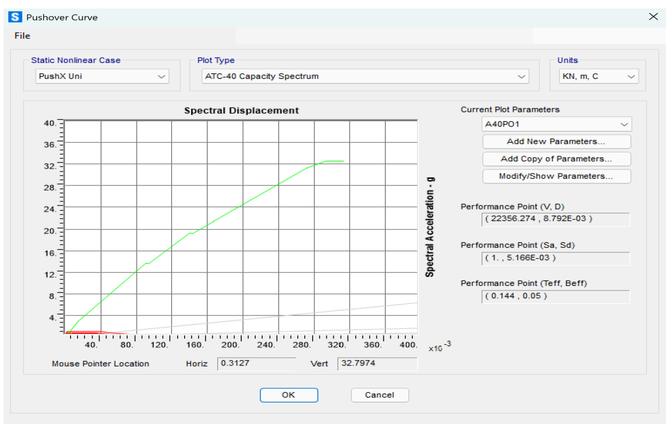

Fig. 86: ATC-40 Curve for PushX Uni G+20 PSW Model

Appendix C – Modal Analysis Results

Model	Fundamental Period (Seconds)	Modal Participation Mass Ratio (%)
G+15 Regular	2.031	94.80
G+20 Regular	2.837	96.23
G+20 Irregular	2.071	94.09
G+20 CSW	1.32	95.43
G+20 PSW	1.602	96.30

Appendix D - Capacity Curves for Load Cases in Y-directions

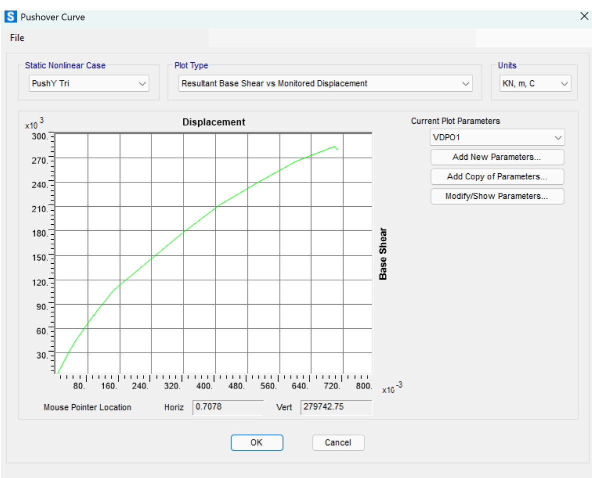

Fig. 87: PushY Parabolic CC for G+15

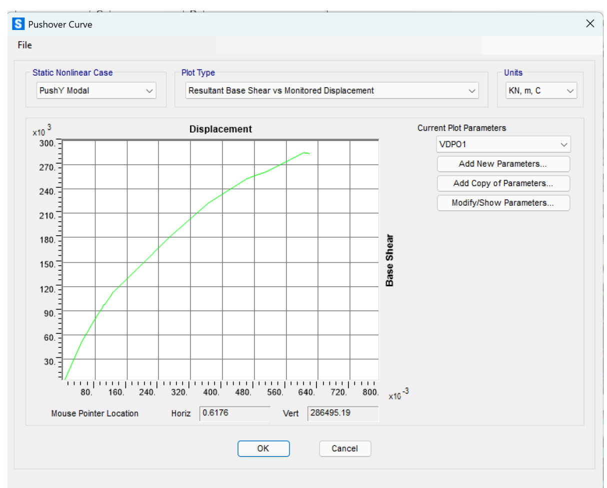

Fig. 88: PushY Modal CC for G+15

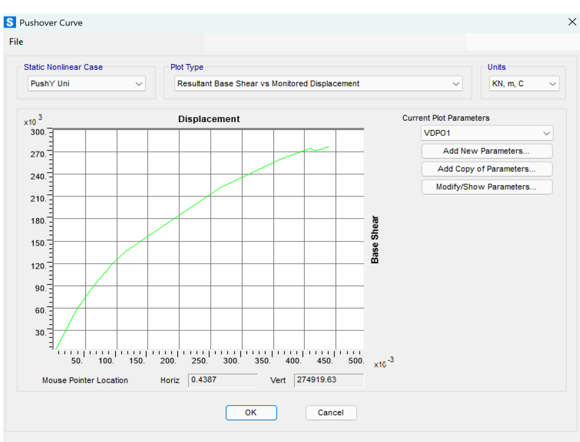

Fig. 89: PushY Uniform CC for G+15

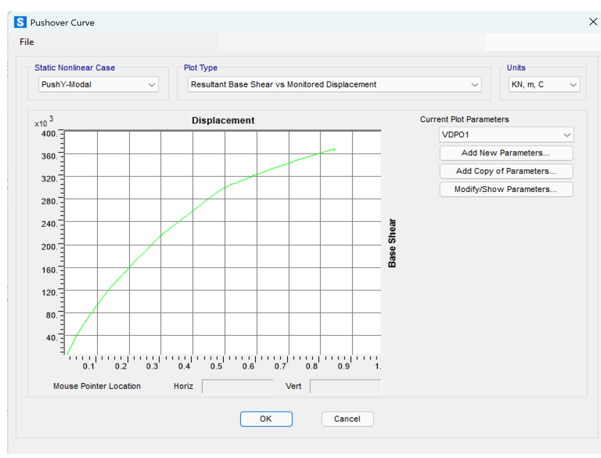

Fig. 90: PushY Modal CC for G+20

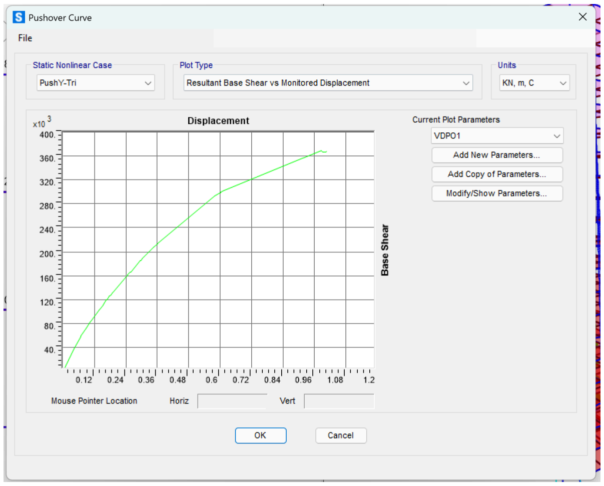

Fig. 91: PushY Parabolic CC for G+20

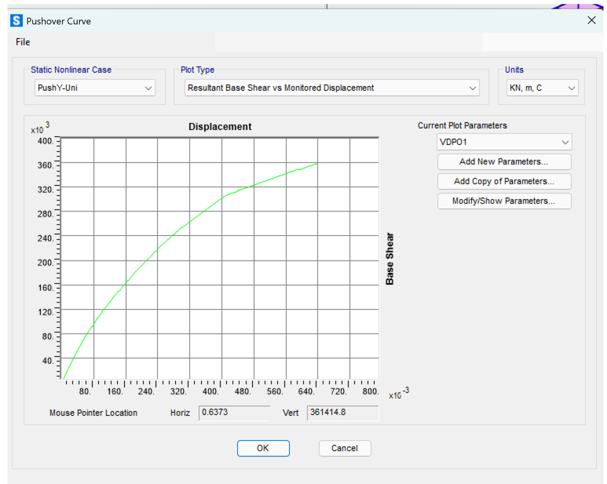

Fig. 92: PushY Uniform CC for G+20

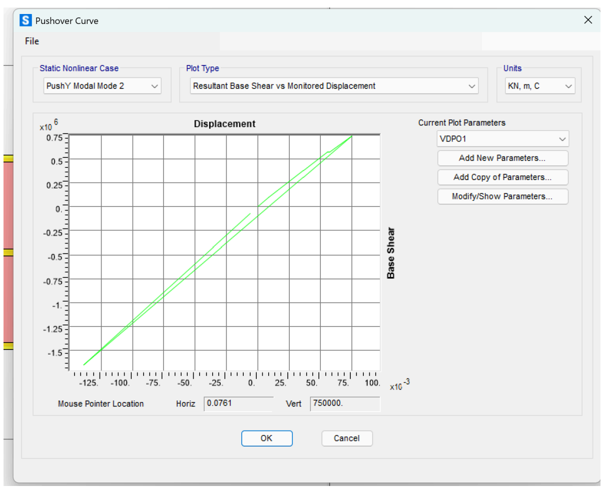

Fig. 93: PushY Modal CC for G+20 CSW

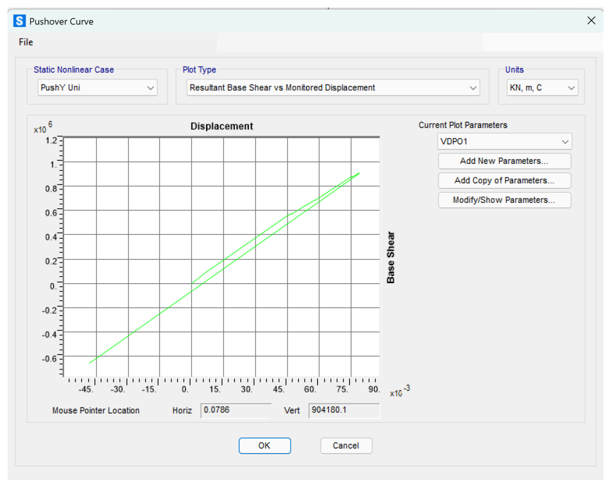

Fig. 94: PushY Uniform CC for G+20 CSW

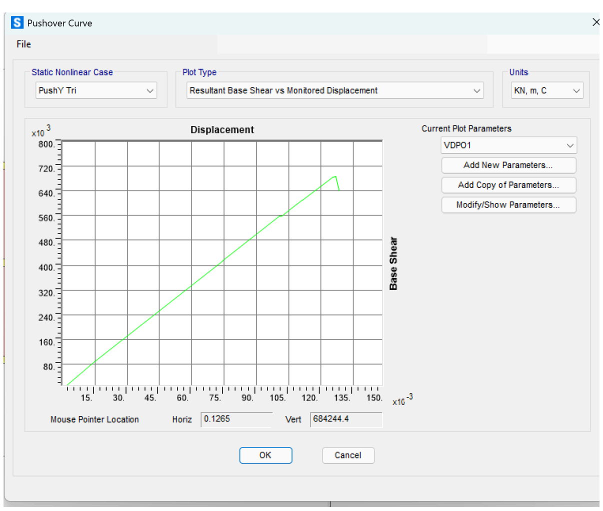

Fig. 95: PushY Parabolic CC for G+20 CSW

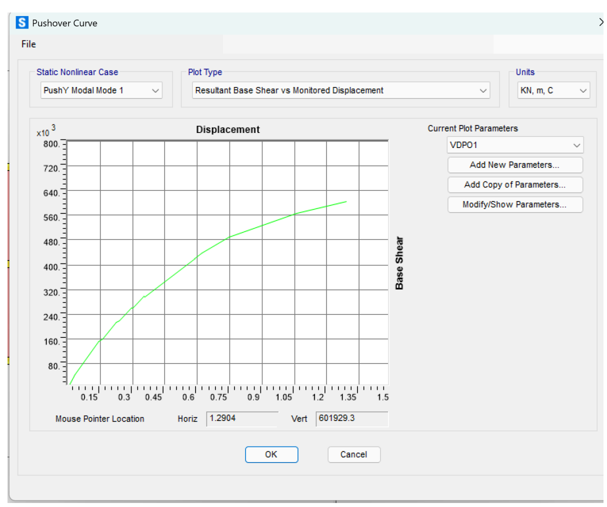

Fig. 96: PushY Modal CC for G+20 Irregular

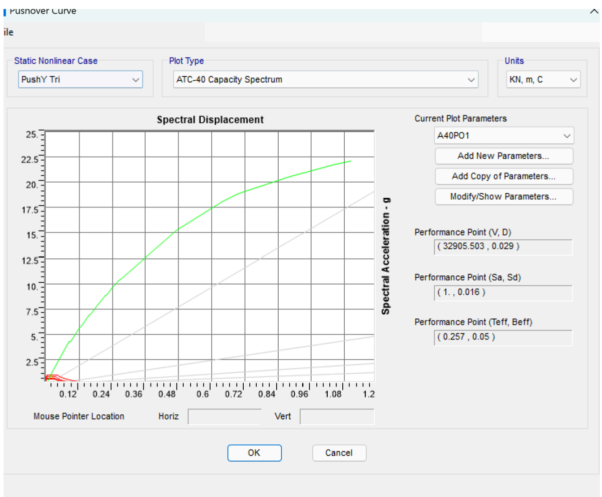

Fig. 97: PushY Parabolic CC for G+20 Irregular

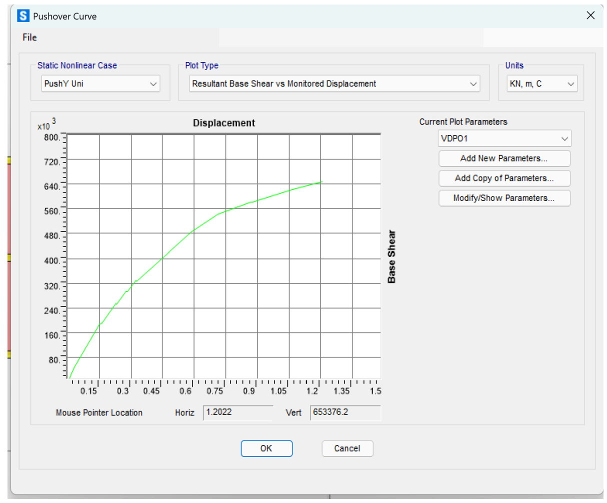

Fig. 98: PushY Uniform CC for G+20 Irregular

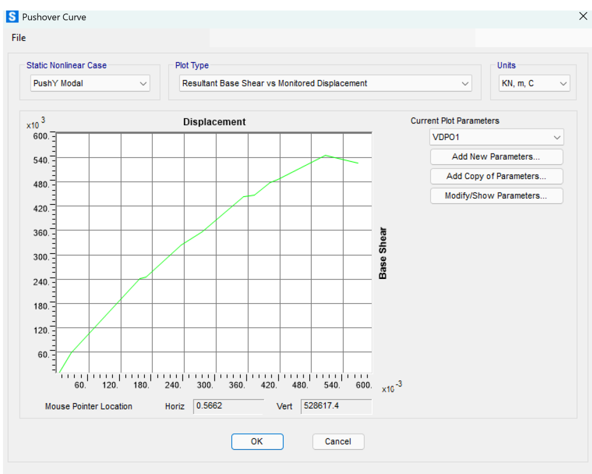

Fig. 99: PushY Modal CC for G+20 PSW

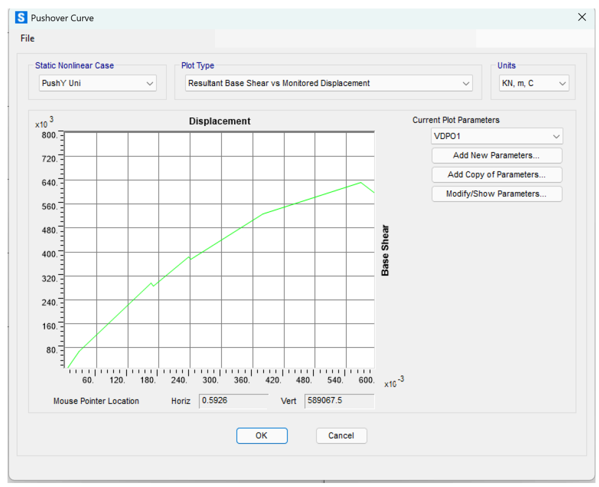

Fig. 100: PushY Uniform CC for G+20 PSW

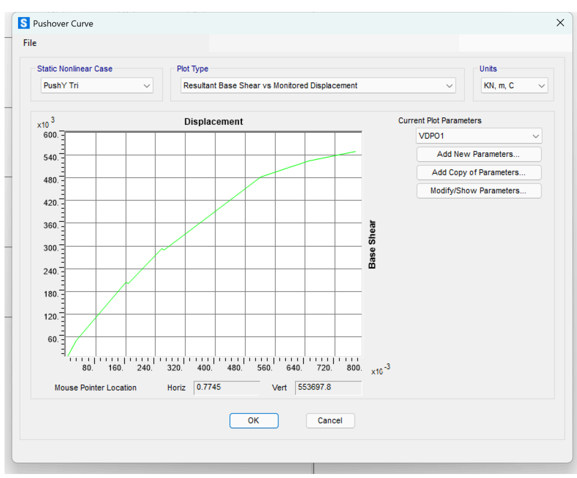

Fig. 101: PushY Parabolic CC for G+20 PSW